RESEARCH ARTICLE

Multiple pathways of toxicity induced by *C9orf72* dipeptide repeat aggregates and G_4C_2 RNA in a cellular model

Frédéric Frottin[1,2]*, Manuela Pérez-Berlanga[1,3], F Ulrich Hartl[1]*, Mark S Hipp[1,4,5]*

[1]Max Planck Institute of Biochemistry, Martinsried, Germany; [2]Université Paris-Saclay, CEA, CNRS, Institute for Integrative Biology of the Cell (I2BC), Gif-sur-Yvette, France; [3]Department of Quantitative Biomedicine, University of Zurich, Zurich, Switzerland; [4]Department of Biomedical Sciences of Cells and Systems, University Medical Center Groningen, University of Groningen, Groningen, Netherlands; [5]School of Medicine and Health Sciences, Carl von Ossietzky University Oldenburg, Oldenburg, Germany

Abstract The most frequent genetic cause of amyotrophic lateral sclerosis and frontotemporal dementia is a G_4C_2 repeat expansion in the *C9orf72* gene. This expansion gives rise to translation of aggregating dipeptide repeat (DPR) proteins, including poly-GA as the most abundant species. However, gain of toxic function effects have been attributed to either the DPRs or the pathological G_4C_2 RNA. Here, we analyzed in a cellular model the relative toxicity of DPRs and RNA. Cytoplasmic poly-GA aggregates, generated in the absence of G_4C_2 RNA, interfered with nucleocytoplasmic protein transport, but had little effect on cell viability. In contrast, nuclear poly-GA was more toxic, impairing nucleolar protein quality control and protein biosynthesis. Production of the G_4C_2 RNA strongly reduced viability independent of DPR translation and caused pronounced inhibition of nuclear mRNA export and protein biogenesis. Thus, while the toxic effects of G_4C_2 RNA predominate in the cellular model used, DPRs exert additive effects that may contribute to pathology.

***For correspondence:**
frederic.frottin@i2bc.paris-saclay.fr (FF);
uhartl@biochem.mpg.de (FUH);
m.s.hipp@umcg.nl (MSH)

Competing interest: See page 18

Funding: See page 18

Received: 02 September 2020
Accepted: 08 June 2021
Published: 23 June 2021

Reviewing editor: Susan L Ackerman, Howard Hughes Medical Institute, University of California, San Diego, United States

Introduction

Expansion of a GGGGCC hexanucleotide repeat (hereafter G_4C_2) within the first intron of the *C9orf72* gene is the most frequent genetic cause of amyotrophic lateral sclerosis (ALS) and frontotemporal dementia (FTD) (***DeJesus-Hernandez et al., 2011***; ***Renton et al., 2011***). Mutant *C9orf72* in patients suffering from ALS/FTD can have more than a thousand G_4C_2 repeats, while healthy individuals possess usually less than 20 repeats (***Gijselinck et al., 2016***; ***Nordin et al., 2015***). Transcripts with expanded G_4C_2 tracts are translated by repeat associated non-AUG (RAN) translation in all reading frames and in both strands, resulting in the synthesis of five different dipeptide repeat proteins (DPRs): poly-GA, poly-GR, poly-GP, poly-PR, and poly-PA (***Ash et al., 2013***; ***Gendron et al., 2013***; ***Mackenzie et al., 2015***; ***Mori et al., 2013a***; ***Mori et al., 2013c***; ***Zu et al., 2013***), all of which have been detected in patient brains (***Mori et al., 2013a***; ***Mori et al., 2013c***; ***Zu et al., 2013***). Poly-GA is the most abundant of the DPRs, followed by the other sense strand-encoded forms (poly-GP and poly-GR) (***Mackenzie et al., 2015***; ***Mori et al., 2013c***; ***Schludi et al., 2015***). In patient brain and cellular models, DPRs accumulate in deposits that can be found in the nucleus and cytoplasm, including neurites (***Ash et al., 2013***; ***Gendron et al., 2013***; ***Mackenzie et al., 2015***; ***Mori et al., 2013a***; ***Mori et al., 2013c***; ***Schludi et al., 2015***; ***Zu et al., 2013***). Poly-GA aggregates are localized mainly in the cytoplasm (***Davidson et al., 2016***; ***Lee et al., 2017***; ***Mackenzie et al., 2015***; ***Zhang et al., 2016***), whereas arginine-containing DPRs (R-DPRs; poly-GR and poly-PR) accumulate in the nucleus

(**Mackenzie et al., 2015**; **Schludi et al., 2015**). R-DPRs have also been shown in cellular models to localize to the nucleolus (**Kwon et al., 2014**; **Lee et al., 2017**; **May et al., 2014**; **Moens et al., 2019**; **Wen et al., 2014**; **White et al., 2019**; **Yamakawa et al., 2015**; **Zhang et al., 2014**). However, in patients, poly-GR and poly-PR predominantly form cytoplasmic deposits, with only a fraction of cells containing para-nucleolar inclusions that co-localize with silent DNA (**Mackenzie et al., 2015**; **Schludi et al., 2015**). Interestingly, the less frequent intranuclear poly-GA inclusions in both cell models and patient brain are excluded from the nucleoli (**Schludi et al., 2015**).

Both loss- and gain-of-function mechanisms have been suggested to contribute to *C9orf72* pathology (reviewed in **Balendra and Isaacs, 2018**; **Jiang and Ravits, 2019**; **Swinnen et al., 2018**). Despite its location in a non-coding part of the gene, the G_4C_2 expansion can alter the expression level of the C9ORF72 protein (**Rizzu et al., 2016**; **Shi et al., 2018**; **Waite et al., 2014**). However, *C9orf72* knockout mouse models failed to fully recapitulate ALS- or FTD-related neurodegenerative phenotypes, suggesting that loss of C9ORF72 protein is not the only contributor to pathology (**Atanasio et al., 2016**; **Burberry et al., 2016**; **Burberry et al., 2020**; **Jiang et al., 2016**; **Koppers et al., 2015**; **Lagier-Tourenne et al., 2013**; **O'Rourke et al., 2016**; **Panda et al., 2013**; **Sudria-Lopez et al., 2016**; **Sullivan et al., 2016**; **Suzuki et al., 2013**; **Ugolino et al., 2016**; **Zhu et al., 2020**).

Toxic functions induced by the G_4C_2 expansion have been studied in various cellular and animal models, and both RNA- and protein-based mechanisms of toxicity have been proposed (**Arzberger et al., 2018**). However, the main contributor to gain of toxic function in the disease remains to be defined. Pathological G_4C_2 mRNA forms stable G-quadruplexes in the nucleus that retain RNA binding proteins and induce splicing defects (**Cooper-Knock et al., 2014**; **Donnelly et al., 2013**; **Gitler and Tsuiji, 2016**; **Haeusler et al., 2014**; **Sareen et al., 2013**; **Simón-Sánchez et al., 2012**; **Xu et al., 2013**), but has also been observed in the cytoplasm (**Cooper-Knock et al., 2015**; **Liu et al., 2016**; **Mizielinska et al., 2017**; **Ohki et al., 2017**; **Swinnen et al., 2018**). G_4C_2-containing RNA and associated DPRs have been reported to alter the nucleocytoplasmic transport machinery (**Boeynaems et al., 2016**; **Freibaum et al., 2015**; **Jovičić et al., 2015**; **Zhang et al., 2015**). Moreover, R-DPRs can interact with membrane-free phase-separated compartments, such as the nucleolus, causing nucleolar stress and dysfunction of nucleolar quality control, impairment of nucleocytoplasmic trafficking and protein translation, as well as induction of stress granule formation (**Frottin et al., 2019**; **Hayes et al., 2020**; **Kanekura et al., 2016**; **Kwon et al., 2014**; **Lee et al., 2016**; **Mizielinska et al., 2017**; **Moens et al., 2019**; **Radwan et al., 2020**; **Shi et al., 2017**; **Tao et al., 2015**; **Vanneste et al., 2019**; **White et al., 2019**; **Yamakawa et al., 2015**; **Zhang et al., 2018b**). Additionally, cytoplasmic poly-GA aggregates associate extensively with proteasomes and other components of the ubiquitin proteasome system, and interfere with proteasome activity (**Al-Sarraj et al., 2011**; **Guo et al., 2018**; **Khosravi et al., 2020**; **May et al., 2014**; **Mori et al., 2013c**; **Riemslagh et al., 2019**), as well as induce mislocalization of nuclear proteins (**Khosravi et al., 2017**; **Nihei et al., 2020**; **Nonaka et al., 2018**; **Solomon et al., 2018**). In mice expressing poly-GA, the aggregates have also been observed to sequester nuclear pore components (**Zhang et al., 2016**), thereby interfering with nucleocytoplasmic protein transport. In light of these studies, it seems likely that multiple toxicity mechanisms contribute to pathogenesis (**Balendra and Isaacs, 2018**).

Here, we used G_4C_2 repeat-containing constructs as well as synthetic DPR constructs not generating G_4C_2 RNA to analyze the relative contributions of RNA and DPR species to pathology in a cellular model. The mRNA and protein constructs analyzed were of equivalent length. By retaining DPR proteins in the cytoplasm or targeting them to the nucleus, we found that cytoplasmic, but not nuclear poly-GA, aggregates impaired nucleocytoplasmic transport. However, a direct comparison of length-matched constructs showed that nuclear poly-GA was more toxic and interfered with nucleolar protein quality control and protein synthesis. Importantly, by leveraging the finding that cytoplasmic poly-GA does not induce toxicity in the cellular model system, we were able to isolate the contribution of the G_4C_2 repeat RNA to cellular pathology. The G_4C_2-containing RNA species induced a strong accumulation of poly-adenylated mRNA within the nucleus and dramatically inhibited protein biosynthesis. Thus, poly-GA protein and G_4C_2 RNA interfere with multiple key cellular pathways, with the RNA component exerting the major toxic effects limiting cell viability.

Results

Nuclear and cytoplasmic poly-GA aggregates differ in toxicity

Both G_4C_2 RNA and DPR proteins resulting from the pathological *C9orf72* expansion have been suggested to mediate gain of toxic function effects in various models (reviewed in ***Balendra and Isaacs, 2018***). To investigate the contribution of poly-GA proteins to cellular pathology, we engineered ATG-driven synthetic constructs expressing 65 GA repeats fused C-terminally to GFP (GA_{65}-GFP). Notably, these constructs do not contain any G_4C_2 hexanucleotide motifs (***Figure 1A***, ***Figure 1—figure supplement 1A***).

Expression of GA_{65}-GFP in HEK293 cells resulted in the formation of bright fluorescent inclusions in most transfected cells. The inclusions were generally cytoplasmic, except for a small fraction of cells with nuclear foci (***Figure 1B***). This phenotype is consistent with reports on the localization of poly-GA aggregates in patient brain, where poly-GA aggregates are also observed in the neuronal

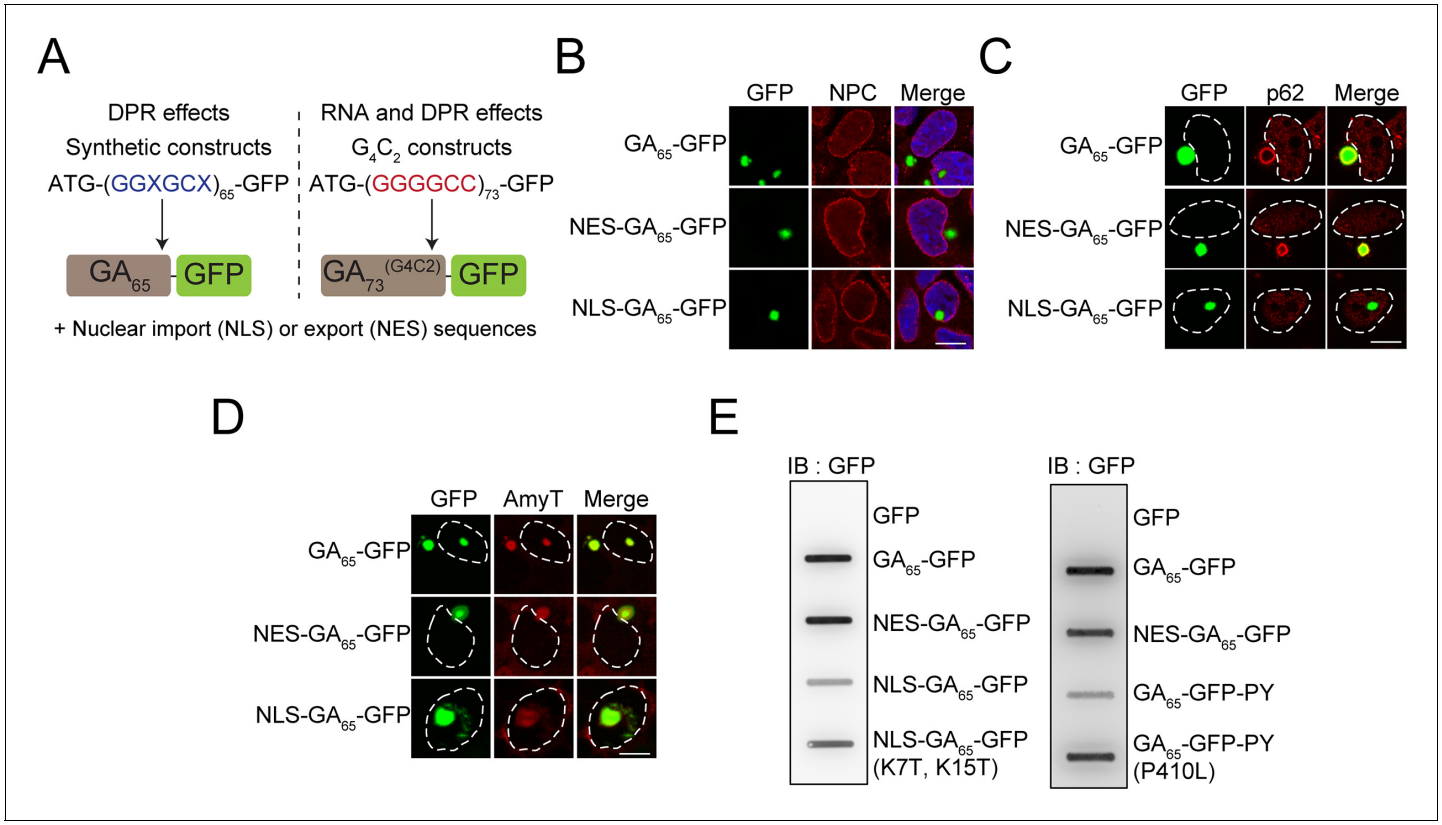

Figure 1. Cytoplasmic and nuclear poly-GA aggregates are amyloid-like but differ in solubility. (**A**) Schematic representation of the poly-GA encoding constructs used. Two different classes of poly-GA encoding constructs were used to study dipeptide repeat protein (DPR)-mediated toxicity in the presence or absence of RNA repeat regions: synthetic constructs that do not contain G_4C_2 motifs and are translated into GA_{65} (left), and constructs containing 73 G_4C_2 repeats that encode GA_{73} (right). Both classes contained ATG start codons and were fused in frame to GFP. N-terminal nuclear import (NLS) or export sequences (NES) were present when indicated. (**B**) The indicated constructs were transfected into HEK293 cells. Antibodies against nuclear pore complexes (NPC, red) were used to detect the nuclear membrane, poly-GA was visualized by GFP fluorescence (green), and nuclei were counterstained with DAPI. (**C**) NES-GA_{65}-GFP aggregates co-localize with p62. The indicated constructs were transfected into HEK293 cells. p62 (red) was detected by immunofluorescence, and poly-GA was visualized by GFP fluorescence (green). White dashed lines delineate the nucleus based on DAPI staining. (**D**) Cytoplasmic and nuclear aggregates can be stained with an amyloid-specific dye. The indicated constructs were transfected into HEK293 cells and stained with AmyTracker (AmyT, red). Poly-GA DPRs were visualized by GFP fluorescence (green). White dashed lines delineate the nucleus based on DAPI staining. (**E**) Cytoplasmic GA aggregates are SDS insoluble. The indicated constructs were transfected into HEK293 cells. GFP was expressed as a soluble control protein. Cells were lysed and analyzed for SDS-insoluble poly-GA aggregates by filter retardation assay. GFP antibody was used for detection. Scale bars represent 10 µm.

The online version of this article includes the following figure supplement(s) for figure 1:

Figure supplement 1. Cytoplasmic and nuclear poly-GA aggregates differ in their staining properties.

cytoplasm and nucleus (**Mori et al., 2013c**; **Schludi et al., 2015**). Using engineered β-sheet proteins, we have previously reported that otherwise identical aggregation-prone proteins display distinct toxic properties when targeted to different cellular compartments (**Frottin et al., 2019**; **Vincenz-Donnelly et al., 2018**; **Woerner et al., 2016**). To test whether this is also the case for poly-GA, we generated compartment-specific variants of the poly-GA proteins. We restricted the expression of poly-GA to the cytoplasm by adding a nuclear export signal (NES-GA_{65}-GFP) or targeted the protein to the nucleus using a double SV40 nuclear localization signal (NLS-GA_{65}-GFP). NES-GA_{65}-GFP accumulated in the cytoplasm and formed inclusions similar to those of GA_{65}-GFP (**Figure 1B**). Directing the protein to the nucleus resulted in an increased number of cells with nuclear aggregates (**Figure 1B**). However, a number of NLS-GA_{65}-GFP-expressing cells also contained cytoplasmic inclusions, suggesting that aggregate formation in these cells occurred before the transport of the poly-GA proteins into the nucleus.

Poly-GA forms p62-positive inclusions in the cytoplasm of neurons (**Guo et al., 2018**). We were able to replicate this phenotype in our cellular system and observed p62-positive poly-GA inclusions of GA_{65}-GFP and NES-GA_{65}-GFP (**Figure 1C**; **May et al., 2014**; **Mori et al., 2013c**). Both nuclear and cytoplasmic poly-GA inclusions were stained throughout with AmyT, a small amyloid-specific dye (**Figure 1D**). The aggregates were also recognized by the anti-amyloid antibody (OC) (**Figure 1—figure supplement 1B**), which recognizes generic epitopes common to amyloid fibrils and fibrillar oligomers (**Kayed et al., 2007**). However, while the nuclear aggregates stained homogeneously with OC, cytoplasmic GA_{65}-GFP inclusions stained less well and rather showed only a peripheral reaction with the dye (**Figure 1—figure supplement 1B**). The differential antibody accessibility of the inclusion core suggests that the nuclear and cytoplasmic DPR aggregates, though both amyloid-like, differ in structural properties such as packing density.

Analysis of the solubility of the nuclear and cytoplasmic GA_{65}-GFP aggregates supported this interpretation. NES-GA_{65}-GFP was retained in a filter retardation assay in the presence of SDS, while most NLS-GA_{65}-GFP passed through the filter (**Figure 1E**). The difference in detergent solubility was not due to the presence of the NLS sequence since similar results were obtained using the FUS-derived C-terminal nuclear localization signal (PY) (**Gal et al., 2011**; **Figure 1E**). Moreover, disabling of the nuclear targeting sequences by point mutations resulted in the reappearance of SDS-insoluble aggregates (**Figure 1E**). Thus, despite being amyloid-like, nuclear and cytoplasmic poly-GA aggregates have different physico-chemical properties.

The granular component (GC) of the nucleolus has recently been shown to function as a protein quality control compartment (**Frottin et al., 2019**; **Woerner et al., 2016**). Interestingly, the nuclear aggregates of NLS-GA_{65}-GFP altered the localization of the GC marker protein nucleophosmin (NPM1), while cytosolic NES-GA_{65}-GFP had no such effect (**Figure 2A**). Nuclear GA_{65}-GFP aggregates induced the dislocation of NPM1 from the GC phase of the nucleolus, with accumulation of NPM1 at the aggregate periphery (**Figure 2A**). However, the nuclear GA_{65}-GFP deposits did not alter the distribution of the RNA polymerase I subunit RPA40, a marker of the fibrillar center of the nucleolus, the site of rRNA synthesis (**Figure 2B**). The NPM1-containing GC phase is responsible for pre-ribosome particle assembly and also accommodates proteins that have misfolded upon stress. These proteins enter the GC phase and are maintained in a state competent for refolding and repartitioning to the nucleoplasm upon recovery from stress (**Frottin et al., 2019**). In contrast to poly-GA, R-DPRs enter the GC phase of the nucleolus and convert it from liquid-like to a more hardened state, thereby impairing its quality control function (**Frottin et al., 2019**; **Lee et al., 2016**). To test whether nuclear poly-GA aggregates also affect nucleolar quality control, we expressed the synthetic poly-GA constructs in HEK293 cells together with nuclear firefly luciferase fused to the red fluorescent protein mScarlet (NLS-LS), a metastable protein that enters the GC phase upon stress-induced misfolding (**Frottin et al., 2019**). In control cells, NLS-LS accumulated in the nucleolus upon heat stress and largely repartitioned to the nucleoplasm within 2 hr of recovery (**Figure 2C**, **Figure 2—figure supplement 1A**). A similar result was obtained upon expression of cytoplasmic NES-GA_{65}-GFP. However, in the presence of aggregates of NLS-GA_{65}-GFP, NLS-LS failed to efficiently repartition to the nucleoplasm (**Figure 2C**, **Figure 2—figure supplement 1A**), indicating that the nuclear poly-GA aggregates compromise nucleolar protein quality control.

We next analyzed the viability of HEK293 cells expressing poly-GA in cytoplasm or nucleus. We used the MTT assay to measure metabolic activity, which reflects not only cytotoxic effects but also changes in cell division and overall cellular fitness. Cytoplasmic and nuclear forms of an

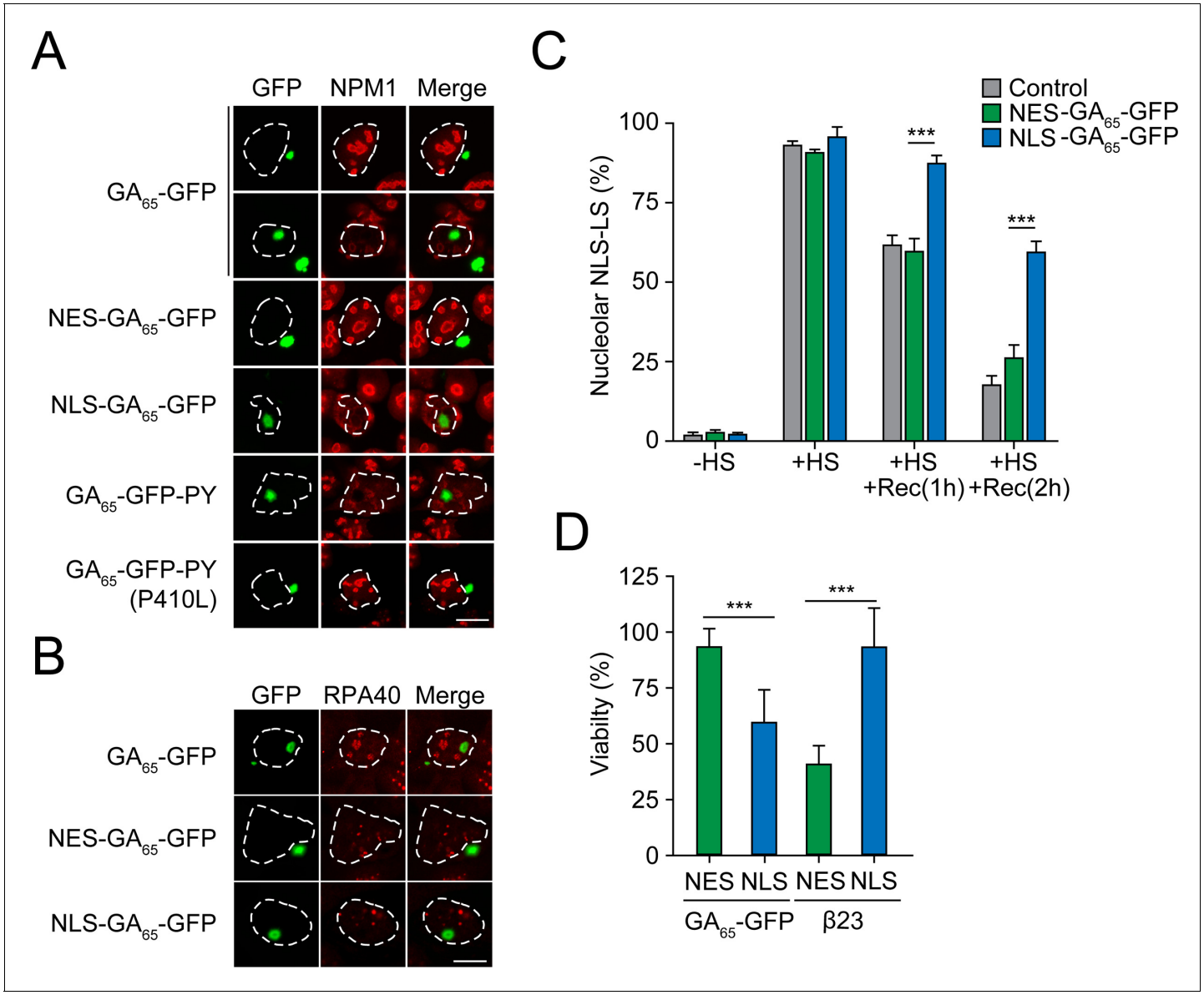

Figure 2. Nuclear poly-GA aggregates compromise nucleolar integrity and impair cell viability. (**A**) Nuclear poly-GA aggregates alter nucleophosmin (NPM1) localization. The indicated constructs were transfected into HEK293 cells. Cells were fixed and stained with anti-NPM1 antibodies (red). Poly-GA was visualized by GFP fluorescence (green). (**B**) Nuclear poly-GA aggregates are not nucleolar. The indicated constructs were transfected into HEK293 cells, followed by staining with antibodies against DNA-directed RNA polymerases I and III subunit RPAC1 (RPA40) (red). Poly-GA was visualized by GFP fluorescence (green). (**C**) Nuclear poly-GA aggregates disrupt nucleolar protein quality control. HEK293 cells were co-transfected with NLS-firefly luciferase fused to mScarlet (NLS-LS) and the indicated poly-GA constructs or GFP as a control. Cells were maintained at 37˚C (–HS) or subjected to heat stress 43˚C (+HS) for 2 hr or heat stress and recovery (+HS + Rec) for 1 hr and 2 hr. Cells with nucleolar NLS-LS were counted, and the results plotted as percentage of transfected cells. Data are shown as mean + SD (n = 3). p-Value of two-sided t-test is displayed (***p≤0.001). Representative immunofluorescence images are shown in ***Figure 2—figure supplement 1A***. (**D**) Nuclear poly-GA is toxic. HEK293 cells were transfected with the indicated constructs, and MTT cell viability assays were performed 4 days after transfection. Data were normalized to cells transfected with empty vector. Data are shown as means + SD (n ≥ 3); p-values of two-sided t-test are shown (***p≤0.001). White dashed lines delineate the nucleus based on DAPI staining. Scale bars represent 10 μm.

The online version of this article includes the following source data and figure supplement(s) for figure 2:

Source data 1. Numerical values for graph in ***Figure 2C***.
Source data 2. Numerical values for graph in ***Figure 2D***.
Figure supplement 1. Nuclear poly-GA aggregates impair nucleolar protein quality control and cell viability.

amyloidogenic model protein without repeat sequences (β23) served as a control (***West et al., 1999***; ***Woerner et al., 2016***). While the expression of NES-GA_{65}-GFP did not cause toxicity, metabolic activity was significantly reduced upon expression of NLS-GA_{65}-GFP (***Figure 2D***). This effect was reproduced in cells transfected with a plasmid coding for GA_{65} from an alternative degenerated and G_4C_2-free DNA sequence (GA_{65}(2)) (***Figure 1—figure supplement 1A***, ***Figure 2—figure supplement 1B***), further excluding RNA-mediated toxicity. Decreased viability was also observed when GA_{65}-GFP was targeted to the nucleus via the alternative PY localization signal (***Figure 2—figure***

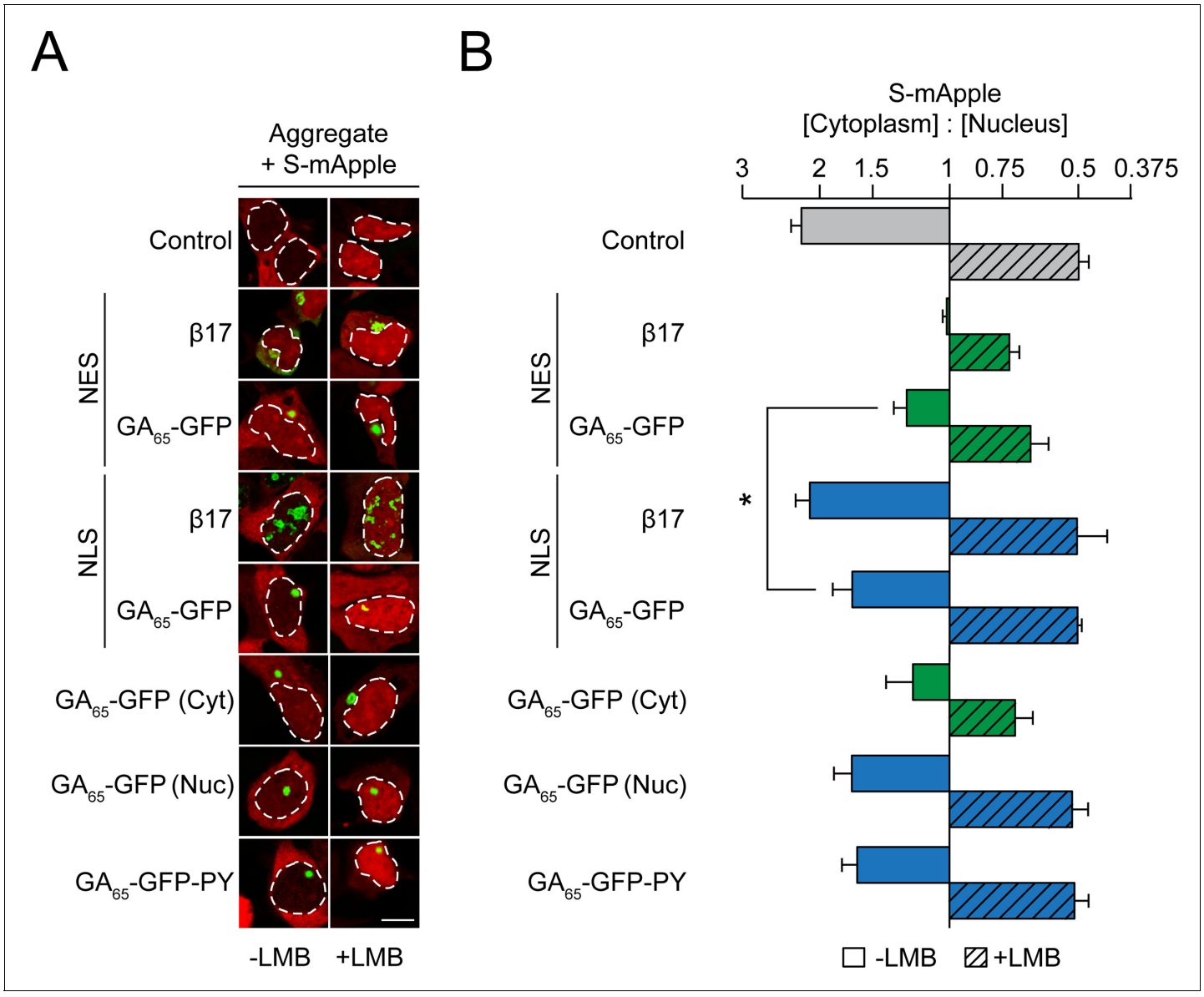

Figure 3. Cytoplasmic poly-GA aggregates impair nucleocytoplasmic protein transport. (**A**) Cytoplasmic poly-GA aggregates alter nuclear transport of a shuttling reporter protein. HEK293 cells were co-transfected with S-mApple (red) and either empty vector (Control), NES-β17, NES-GA_{65}-GFP, NLS-β 17, NLS-GA_{65}-GFP, GA_{65}-GFP, or GA_{65}-GFP-PY (green). Leptomycin B (LMB; 10 ng/ml) was added for 15 min when indicated. White dashed lines delineate nuclei based on DAPI staining. Scale bar represents 10 μm. (**B**) Quantification of S-mApple distribution from data in (**A**). The x-axis shows the enrichment of S-mApple concentration in the cytoplasm relative to the nucleus. Cells transfected with GA_{65}-GFP were further analyzed and divided into cells with cytoplasmic (Cyt) or nuclear (Nuc) aggregates. Data are means + SD, n = 3 independent experiments, >70 cells were analyzed per condition. *$p \leq 0.05$ from two-sided t-test.

The online version of this article includes the following source data for figure 3:

Source data 1. Numerical values for graph in ***Figure 3B***.

supplement 1C). Importantly, both NES-GA_{65}-GFP and NLS-GA_{65}-GFP were expressed at levels comparable to GA_{65}-GFP (*Figure 2—figure supplement 1D*). Point mutations in the NLS or PY targeting sequence prevented accumulation of GA_{65}-GFP in the nucleus and restored viability (*Figure 2—figure supplement 1C*). Together, these results indicate that the difference in toxicity between nuclear and cytoplasmic poly-GA is caused by compartment-specific properties of the aggregates independent of their targeting sequences and mRNA.

Cytoplasmic GA_{65}-GFP aggregates interfere with nuclear transport

We have previously shown that artificial β-sheet proteins, when aggregating in the cytoplasm, sequester nuclear transport factors and thereby interfere with transport of proteins and mRNA across the nuclear envelope (*Woerner et al., 2016*). Similar observations were made for the aggregates of various disease proteins including poly-GA and R-DPRs (*Boeynaems et al., 2016*; *Chou et al., 2018*; *Eftekharzadeh et al., 2019*; *Freibaum et al., 2015*; *Gasset-Rosa et al., 2017*; *Grima et al., 2017*; *Jovičić et al., 2015*; *Khosravi et al., 2017*; *Kramer et al., 2018*; *Solomon et al., 2018*; *Zhang et al., 2015*; *Zhang et al., 2016*). To test which role the localization of the poly-GA proteins plays in this process, we expressed NES-GA_{65}-GFP or NLS-GA_{65}-GFP together with the reporter protein shuttle-mApple (S-mApple). This reporter protein contains both nuclear import and export signals and consequently shuttles between nucleus and cytoplasm. At steady state, S-mApple localized mainly to the cytoplasm, but accumulated within minutes in the nucleus upon inhibition of nuclear export with leptomycin B (LMB) (*Wolff et al., 1997*; *Figure 3*).

As previously described, S-mApple was retained within the nucleus upon expression of the cytoplasmic β-sheet protein NES-β17 (*Figure 3*), indicative of inhibition of nuclear protein export (*Woerner et al., 2016*). Expression of NES-GA_{65}-GFP also impaired S-mApple export from the nucleus (-LMB), but to a lesser extent than NES-β17 (*Figure 3*). A mild impairment of nuclear protein import by NES-GA_{65}-GFP was also observed, as measured upon inhibition of export with LMB (*Figure 3*). As for NLS-β17, nuclear poly-GA aggregates had only a weak effect on protein export (*Figure 3*). Similarly, cells containing nuclear aggregates did not show a significant change in S-mApple import into the nucleus (*Figure 3*). These findings were replicated in cells displaying cytoplasmic or nuclear poly-GA aggregates of untargeted GA_{65}-GFP (*Figure 3*).

We next monitored the nuclear translocation of p65, a subunit of the NF-KB complex, upon stimulation by the cytokine TNFα. In control cells, p65 is largely cytoplasmic and enters the nucleus upon treatment with TNFα (*Figure 4A, B*). Cells containing NES-GA_{65}-GFP aggregates displayed a potent inhibition of p65 translocation (*Figure 4A, B*). A similar effect was seen with cytoplasmic aggregates of polyQ-expanded Huntingtin-exon 1 (Htt96Q) as a positive control (*Figure 4A, B*; *Woerner et al., 2016*). Cells containing cytoplasmic aggregates of untargeted GA_{65}-GFP also displayed reduced p65 translocation (*Figure 4A, B*). The observed translocation impairment was independent of an alteration of p65 phosphorylation and degradation of the inhibitor of nuclear factor κB (IκB) (*Figure 4C*). In contrast, nuclear poly-GA aggregates showed only a limited effect on p65 translocation (*Figure 4A, B*).

Cytoplasmic aggregates of β-sheet model proteins and disease-linked, amyloidogenic proteins cause mislocalization and sequestration of nuclear pore complexes and importins (*Woerner et al., 2016*). Particularly, R-DPRs have also been shown to directly bind and interfere with cargo loading onto importin β at the nuclear pore (*Hayes et al., 2020*). While cytoplasmic poly-GA aggregates had no apparent effect on the localization of the nuclear pore complex (*Figure 1B*), we found that cells with cytoplasmic GA_{65}-GFP aggregates frequently contained aggregate foci of importins α1 (KPNA2) and α3 (KPNA4), as has been observed previously for cytoplasmic aggregates of the aggregation-prone model proteins NES-β23 (*Woerner et al., 2016*). This effect was also observed for importin β1 (KPNB1), although to a lesser degree (*Figure 4—figure supplement 1*). Additionally, importins appeared to be enriched at the periphery of poly-GA inclusions, as seen for KPNA2 and KPNA4 (*Figure 4—figure supplement 1*). Nuclear poly-GA aggregates had no effect on the distribution of these importins (*Figure 4—figure supplement 1*). Thus, similar to the artificial β-sheet proteins, poly-GA aggregates induce compartment-specific cellular defects and impair nucleocytoplasmic protein transport.

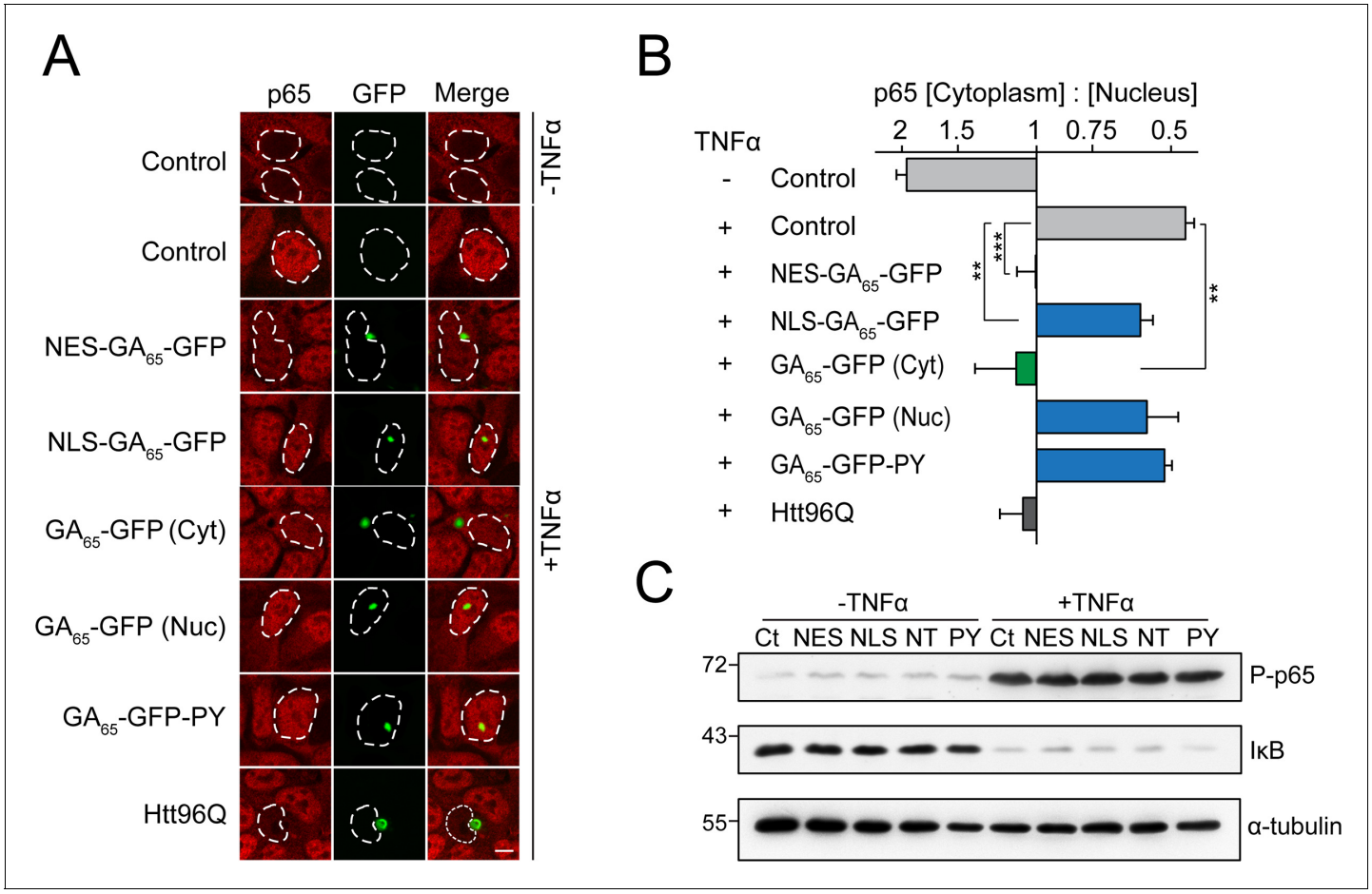

Figure 4. Cytoplasmic poly-GA aggregates inhibit nuclear import of p65. (**A**) Cytoplasmic poly-GA aggregates inhibit p65 nuclear translocation. HEK293 cells were transfected with empty vector (Control), NES-GA_{65}-GFP, NLS-GA_{65}-GFP, GA_{65}-GFP, GA65-GFP-PY, or Htt96Q-GFP (Htt96Q) (green) and analyzed for NF-κB p65 localization (red) with and without TNFα treatment (30 min). White dashed lines delineate nuclei based on DAPI staining. Scale bar represents 10 μm. (**B**) Quantification of NF-κB p65 distribution from data in (**A**). The x-axis shows the enrichment of p65 in the cytoplasm relative to the nucleus. Data are means + SD (n = 3), >100 cells were analyzed per condition. **p≤0.01, ***p≤0.001 from two-sided t-test. (**C**) Expression of poly-GA does not alter the degradation of IκB and phosphorylation of p65. HEK293 cells were transfected with the indicated constructs (Ct: Control; NES: NES-GA_{65}-GFP; NLS: NLS-GA_{65}-GFP; NT: GA_{65}-GFP; PY: GA_{65}-GFP-PY) and treated as described in (**A**). Levels of IκB and phosphorylated NF-κB p65 (P–p65) were analyzed by immunoblotting. α-tubulin served as loading control.
The online version of this article includes the following source data and figure supplement(s) for figure 4:

Source data 1. Numerical values for graph in ***Figure 4B***.
Figure supplement 1. Importins form aggregates in cells containing cytoplasmic poly-GA aggregates and are partially sequestered.

G_4C_2 repeat mRNA causes nuclear mRNA retention and pronounced toxicity

An aberrant distribution of mRNA has been observed in mouse motor neuron-like cells expressing expanded G_4C_2 repeats and in *C9orf72* patient cortical neurons (***Freibaum et al., 2015***; ***Rossi et al., 2015***). We used an oligo-dT probe to test whether cytoplasmic poly-GA aggregates, generated from constructs lacking G_4C_2, affect the cellular distribution of total mRNA. In control cells, mRNA was present throughout the cytoplasm and in small nuclear ribonucleic particles (***Figure 5A***; ***Carter et al., 1991***). Expression of NES-GA_{65}-GFP had only a minor effect on cellular mRNA distribution (***Figure 5A, B***), in contrast to the expression of cytoplasmic β-protein (NES-β17), which resulted in pronounced nuclear mRNA retention (***Woerner et al., 2016***). Likewise, NLS-GA_{65}-GFP only caused limited mRNA retention in the nucleus (***Figure 5A, B***). Thus, poly-GA aggregates interfere with the function of only a subset of nuclear transport factors.

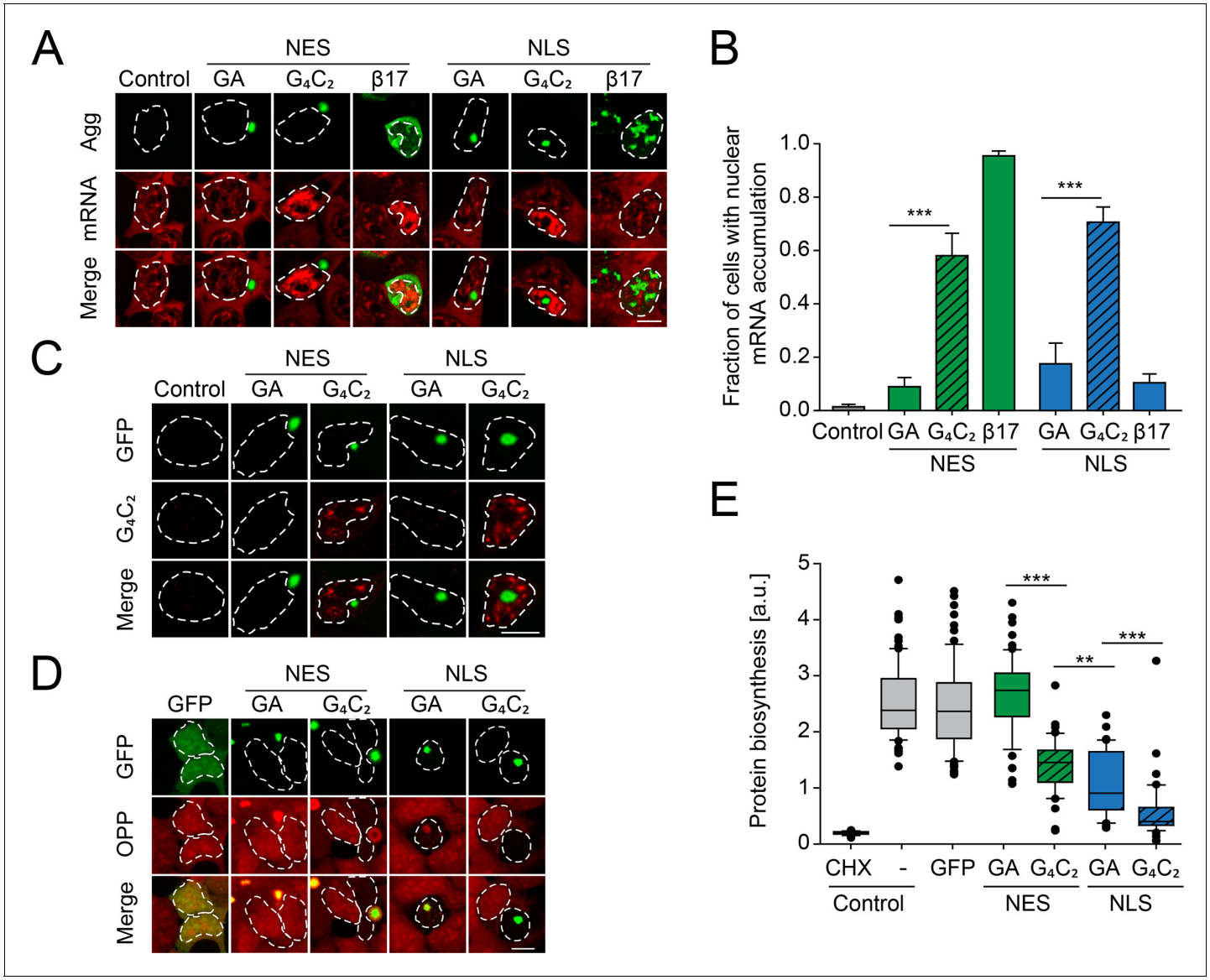

Figure 5. Protein biosynthesis defects correlate with retention of mRNA in the nucleus induced by G_4C_2 mRNA as well as presence of nuclear poly-GA aggregates. (**A**) G_4C_2-containing constructs induce strong nuclear mRNA accumulation. HEK293 cells were transfected with the indicated constructs: empty vector (Control); NES-GA_{65}-GFP (NES-GA); NES-G_4C_2-GFP (NES-G_4C_2); NES-β17; NLS-GA_{65}-GFP (NLS-GA); NLS-G_4C_2-GFP (NLS-G_4C_2); NLS-β17. PolyA-RNA was detected by fluorescence in situ hybridization using a poly-dT probe (red); protein aggregates (Agg) green. (**B**) Quantification of data in (**A**). The graph shows the fraction of cells with nuclear mRNA accumulation. Data are means + SD (n = 3), ***p≤0.001 from two-sided t-test. (**C**) G_4C_2-containing constructs induce the formation of G_4C_2 RNA foci. HEK293 cells were transfected with the indicated constructs: empty vector (Control); NES-GA_{65}-GFP (NES-GA); NES-G_4C_2-GFP (NES-G_4C_2); NLS-GA_{65}-GFP (NLS-GA); NLS-G_4C_2-GFP (NLS-G_4C_2). Cells were analyzed for GFP fluorescence (green) and C_4G_2 fluorescence by in situ hybridization (red). (**D**) Decreased protein biosynthesis in the presence of nuclear poly-GA and G_4C_2 mRNA. Newly synthesized proteins were labeled with O-propargyl-puromycin (OPP; red) in HEK293 cells transfected with the indicated constructs (green). The white dashed lines delineate the nucleus based on DAPI staining, and the scale bar represents 10 μm. (**E**) Quantification of data in (**D**). Analysis of control cells transfected with empty vector and treated with the translation inhibitor cycloheximide (CHX) when indicated is included as control. Boxplot of a representative experiment is shown. Center lines show the medians; box limits indicate the 25th and 75th percentiles; whiskers extend to the 10th and 90th percentiles, outliers are plotted as circles. Welch's t-test was used to assess statistical significance (**p≤0.01; ***p≤0.001).
The online version of this article includes the following source data and figure supplement(s) for figure 5:

Source data 1. Numerical values for graph in ***Figure 5B***.
Source data 2. Numerical values for repeats for ***Figure 5E***.
Figure supplement 1. Expression of G_4C_2-containing constructs induces mRNA retention in the nucleus.

Given that expression of poly-GA protein alone did not recapitulate the alterations of mRNA localization observed in *C9orf72* patient brain (**Freibaum et al., 2015**; **Rossi et al., 2015**), we next analyzed the effect of an ATG-driven poly-GA construct of 73 GA repeats encoded entirely by G_4C_2 motifs $(G_4C_2)_{73}$ (**Figure 1A, Figure 1—figure supplement 1A**). Comparable to the synthetic GA_{65}-GFP sequences, these constructs also generated poly-GA protein aggregates in the cytoplasm or nucleus (**Figure 5A, C**). Importantly, as cytoplasmic poly-GA did not induce toxicity in our cell system, the use of NES and NLS targeting sequences allowed us to isolate the contribution of the G_4C_2-containing RNA to cellular pathology. Both NES-$(G_4C_2)_{73}$-GFP and NLS-$(G_4C_2)_{73}$-GFP, besides generating DPR inclusions, resulted in the formation of G_4C_2-positive RNA foci in the nucleus, as observed by fluorescent in situ hybridization (FISH) using a C_4G_2 probe (**Figure 5C**). Cells expressing GA_{65}-GFP or $(G_4C_2)_{73}$-GFP without targeting sequence were analyzed as well, but only the G_4C_2 constructs showed mRNA accumulation in the nucleus of the majority of cells (**Figure 5—figure supplement 1A**). Furthermore, simultaneous visualization of G_4C_2 RNA puncta with the C_4G_2 probe, total mRNA using an oligo-dT probe and GA-GFP revealed that the G_4C_2 RNA foci are associated with nuclear mRNA accumulation, independent of the presence of visible poly-GA protein aggregates (**Figure 5—figure supplement 1B**). Together, these results indicate that G_4C_2 RNA, not poly-GA protein, mediates retention of mRNA in the nucleus.

The nuclear mRNA retention in cells expressing G_4C_2 constructs was accompanied by a marked reduction of protein synthesis as measured by the incorporation of a puromycin derivative into newly translated proteins (**Slomnicki et al., 2016**; **Figure 5D, E**). Interestingly, NLS-GA_{65}-GFP-expressing cells also displayed reduced protein synthesis, independently of G_4C_2 RNA. In contrast, NES-GA_{65}-GFP had no inhibitory effect on protein synthesis (**Figure 5D, E**). Notably, cells expressing NLS-$(G_4C_2)_{73}$-GFP, accumulating both nuclear poly-GA protein and G_4C_2 RNA, were almost completely translation inactive, similar to control cells treated with the translation inhibitor cycloheximide (**Figure 5D, E**). Thus, both nuclear poly-GA protein and G_4C_2 RNA appear to have additive inhibitory effects on protein biosynthesis. We next measured the proliferation rate or viability of cells transiently transfected with either synthetic or G_4C_2-containing constructs. Independent of the presence of a NES or NLS targeting sequence, all G_4C_2 constructs markedly decreased cellular viability (**Figure 6A**), indicating that toxicity was mediated by the expanded G_4C_2 RNA. Moreover, expression of NLS-$(G_4C_2)_{73}$-GFP was more toxic than NLS-GA_{65}-GFP (**Figure 6A**), although the poly-GA levels of the constructs were comparable (**Figure 6—figure supplement 1A**).

Long sequences of repeated G_4C_2 motifs can produce a series of different DPRs by RAN translation (**Ash et al., 2013**; **Gendron et al., 2013**; **Mori et al., 2013a**; **Mori et al., 2013c**; **Zu et al., 2013**). Since the R-DPRs (poly-PR and poly-GR) have been reported to be toxic in cellular models (**Boeynaems et al., 2016**; **Freibaum et al., 2015**; **Lee et al., 2016**; **Shi et al., 2017**; **Tao et al., 2015**; **Zu et al., 2013**), we investigated whether the G_4C_2 constructs produced R-DPRs at levels sufficient to explain the observed toxicity independently of G_4C_2 RNA effects. To this end, we engineered synthetic sequences, resulting in the ATG-driven synthesis of 73 GR or 73 PR repeats (GR_{73}-GFP and PR_{73}-GFP, respectively) without G_4C_2 repeats. GR_{73}-GFP was located predominantly within the cytoplasm and the nucleolus of HEK293 cells, while PR_{73}-GFP accumulated within the nucleoplasm and nucleolus (**Figure 6—figure supplement 1B**), as reported previously (**Frottin et al., 2019**; **Lee et al., 2016**; **May et al., 2014**; **White et al., 2019**). While the expression of $(G_4C_2)_{73}$-GFP dramatically reduced cellular viability, the R-DPRs were not measurably cytotoxic (**Figure 6A**), consistent with an earlier report for constructs with longer repeat lengths (**May et al., 2014**). We used specific anti-GR and anti-PR antibodies to determine the relative accumulation of the R-DPRs in $(G_4C_2)_{73}$-GFP-expressing cells in comparison to cells expressing GR_{73}-GFP and PR_{73}-GFP. The antibodies recognized specific signals in cells transfected with the respective R-DPR constructs, but failed to detect R-DPR protein in cells expressing $(G_4C_2)_{73}$-GFP (**Figure 6B**), indicating that production of R-DPR protein from the G_4C_2 constructs was very inefficient. Given that PR_{73}-GFP and GR_{73}-GFP were produced in detectable quantities from the synthetic constructs without inducing toxicity, we conclude that the pronounced toxicity observed upon expression of $(G_4C_2)_{73}$-GFP cannot be explained by RAN translation of R-DPR but is due to nuclear mRNA retention mediated by the G_4C_2 repeat RNA.

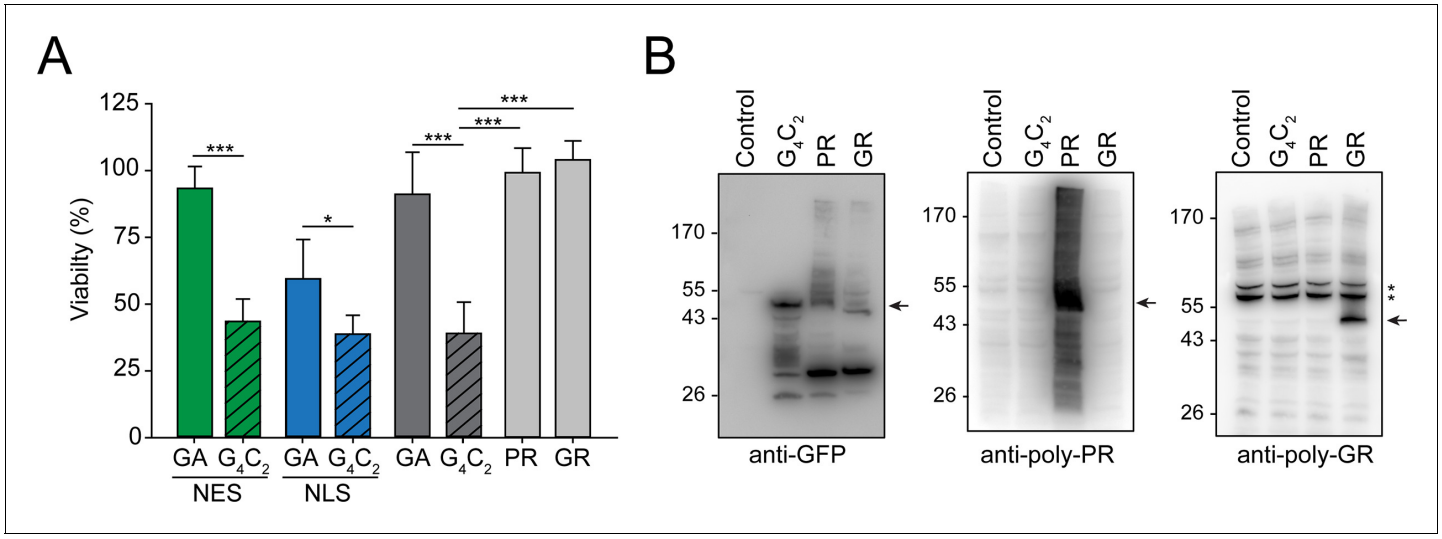

Figure 6. Production of G_4C_2 mRNA strongly decreases cellular viability. (**A**) G_4C_2 mRNA induces strong toxicity. HEK293 cells were transfected with the indicated constructs: G_4C_2-GFP (G_4C_2), NES-G_4C_2-GFP (NES-G_4C_2), NLS-G_4C_2-GFP (NLS-G_4C_2), GA_{65}-GFP (GA), NES-GA_{65}-GFP (NES-GA), NLS-GA_{65}-GFP (NLS-GA), PR_{73}-GFP (PR), or GR_{73}-GFP (GR). MTT cell viability assays were performed 4 days after transfection. Data were normalized to cells transfected with empty vector. Data are means + SD ($n \geq 3$). Part of this data is also shown in ***Figure 2D***. *$p \leq 0.05$; ***$p \leq 0.001$ from two-sided t-test. (**B**) $(G_4C_2)_{73}$-GFP does not produce detectable amounts of arginine containing dipeptide repeats (R-DPRs). HEK293 cells were transfected with the indicated constructs: empty vector (control), $(G_4C_2)_{73}$-GFP (G_4C_2), PR_{73}-GFP (PR), and GR_{73}-GFP (GR). Immunoblot analysis was then performed against GFP (left), poly-PR (center), and poly-GR (right). A representative result of three biological repeats is shown. The arrows indicate the main band of the respective DPRs, and * indicate non-specific bands recognized by the anti-GR antibody.
The online version of this article includes the following source data and figure supplement(s) for figure 6:

Source data 1. Numerical values for graph in ***Figure 6A***.
Figure supplement 1. Expression levels of GA-DPRs and localization of R-DPRs.

Discussion

We have employed a cellular model to differentiate possible mechanisms of toxicity exerted by expansion of the G_4C_2 hexanucleotide tract within the *C9orf72* locus, the most frequent genetic cause of ALS and FTD (***DeJesus-Hernandez et al., 2011***; ***Renton et al., 2011***). Our results demonstrated that the G_4C_2 expansion causes toxicity in our cellular system in a manner dependent on both aggregates of G_4C_2-encoded DPR proteins and the G_4C_2 repeat mRNA. These findings suggest a multiple hit model of additive, but mechanistically independent, effects of proteotoxicity and RNA-mediated toxicity, with the latter being the predominant toxic agent in the model system investigated. However, the longer G_4C_2 expansions, and the resulting DPRs, present in patients may have additional adverse effects that were not recapitulated with the constructs used here.

Both DPRs and repeat mRNA interfered with different aspects of nucleocytoplasmic transport. The G_4C_2 RNA inhibited the export of mRNA from the nucleus, consistent with a dramatic impairment of protein synthesis that would be associated with strong neuronal toxicity. Notably, this effect was independent of the presence of DPR protein aggregates, which is in agreement with results from zebrafish (***Swinnen et al., 2018***), but in contrast to findings observed in *Drosophila* (***Tran et al., 2015***). Additionally, as has been reported for artificial β-sheet proteins and disease-associated aggregation-prone proteins such as Tau, Huntingtin, FUS, and TDP-43 (***Chou et al., 2018***; ***Dormann et al., 2010***; ***Eftekharzadeh et al., 2019***; ***Gasset-Rosa et al., 2017***; ***Grima et al., 2017***; ***Woerner et al., 2016***), cytoplasmic poly-GA aggregates partially inhibited the transport of proteins across the nuclear pore. This observation is in agreement with the previously reported sequestration of a subset of transport factors by poly-GA (***Khosravi et al., 2017***; ***Solomon et al., 2018***; ***Zhang et al., 2016***), and the importin pathology that has been observed in postmortem

frontal cortex tissue of ALS/FTD *C9orf72* patients (**Solomon et al., 2018**). Interestingly, other DPRs have also been reported to inhibit additional aspects of nucleocytoplasmic transport (**Boeynaems et al., 2017**; **Cook et al., 2020**; **Lee et al., 2016**; **Lin et al., 2016**; **Zhang et al., 2018a**). Poly-PR can directly obstruct the central channel of the nuclear pore by binding to the FG domains of nuclear pore proteins (**Shi et al., 2017**), and R-DPRs can disrupt cargo loading onto karyopherins β (**Hayes et al., 2020**).

While the effects of cytoplasmic poly-GA (NES-poly-GA) aggregates on nuclear transport were well tolerated in our cell culture model, poly-GA aggregates within the nucleus (NLS-poly-GA) were associated with substantial proteotoxicity. Nuclear poly-GA formed aggregates at sites that were distinct from nucleoli, similar to the localization of poly-GA aggregates observed in patient brain (**Schludi et al., 2015**). However, formation of these inclusions altered the shape of nucleoli as a result of mislocalization and partial sequestration of the abundant GC protein NPM1, consistent with the nucleolar abnormalities reported in neurons from C9orf72 cases (**Mizielinska et al., 2017**). Nuclear poly-GA aggregates interfered with the recently described protein quality control function of the GC phase of the nucleolus (**Frottin et al., 2019**), as demonstrated using the metastable firefly luciferase as a model substrate. In cells containing nuclear poly-GA aggregates, misfolded luciferase failed to repartition from the nucleolus to the nucleoplasm during recovery from stress. This inhibitory effect was comparable to that previously observed for positively charged DPRs, such as poly-PR, which accumulate directly within the GC phase of the nucleolus (**Frottin et al., 2019**; **Mizielinska et al., 2017**; **Tao et al., 2015**). However, R-DPRs apparently do not accumulate in the nucleolus in patient brain (**Mackenzie et al., 2015**; **Schludi et al., 2015**), and thus may rather interfere with nucleolar quality control by the mechanism described here for nuclear poly-GA (**Frottin et al., 2019**; **Kwon et al., 2014**; **White et al., 2019**).

Expression of poly-GA from G_4C_2-containing constructs resulted in substantially greater toxicity than expression from synthetic constructs when similar poly-GA lengths and amounts were compared. The G_4C_2 hexanucleotide repeat is thought to exert toxic effects in part by forming higher-order RNA assemblies in the nucleus that sequester RNA-binding proteins (**Almeida et al., 2013**; **Cooper-Knock et al., 2015**; **Cooper-Knock et al., 2014**; **Donnelly et al., 2013**; **Haeusler et al., 2014**; **Mori et al., 2013b**; **Reddy et al., 2013**; **Rossi et al., 2015**; **Sareen et al., 2013**; **Xu et al., 2013**). Even if longer G_4C_2 sequences may mediate additional effects (**West et al., 2020**), the G_4C_2 constructs tested here resulted in a pronounced inhibition of protein synthesis, even when coding for cytoplasmic poly-GA protein (NES-GA_{65}), which did not impair protein biogenesis when produced from a synthetic (non-$G_4C_{2)}$ construct. However, because expression constructs based on G_4C_2 repeats also generate the different RAN translation DPR products, a clear distinction between RNA and DPR toxicity in previous studies had been difficult. We therefore compared not only the relative toxicity of poly-GA and G_4C_2 constructs, but also measured the toxicity of poly-PR and poly-GR constructs in the absence of G_4C_2 repeat RNA. Notably, expression of these protein-only constructs did not induce overt toxicity even when expressed at levels much higher than those generated by RAN translation of the G_4C_2 repeat. These findings allowed us to unequivocally attribute the major component of toxicity associated with G_4C_2 constructs to the production of the pathological G_4C_2 RNA sequence. Although DPRs may be undetectable in the brain regions most affected by neurodegeneration in *C9orf72* patients (**Schludi et al., 2015**), we cannot exclude a DPR contribution to pathology in carriers of G_4C_2 expansions, where combinations of the various DPRs and mRNA are present simultaneously, and nondividing cells are exposed to these factors for extended time periods. Indeed, nuclear poly-GA also interfered with protein biosynthesis, presumably by impairing the nucleolar function in ribosome biogenesis, and thus could enhance the toxic effects of G_4C_2 repeat RNA.

In summary, our results indicate that the G_4C_2 expansion in *C9orf72* interferes with multiple nuclear functions, culminating in an inhibition of protein biogenesis, an outcome that would be especially harmful to neuronal cells. These dominant toxic effects might be further aggravated by a loss of function of the endogenous C9ORF72 protein, which is thought to play a role in cellular quality control (**Boivin et al., 2020**; **Sellier et al., 2016**; **Sullivan et al., 2016**; **Yang et al., 2016**; **Zhu et al., 2020**). Further research on the relative contribution of the different toxic mechanisms will be important in developing therapeutic strategies.

Materials and methods

Key resources table

Reagent type (species) or resource	Designation	Source or reference	Identifiers	Additional information
Cell line (*Homo sapiens*, female)	HEK293	ATCC	Cat. #: ATCC-CRL-1573 RRID:CVCL_0045	Lot/Batch No: 63777489
Recombinant DNA reagent	pcDNA3.1 GA_{65}-GFP	This paper		Described in Results part 1 and Materials and methods section
Recombinant DNA reagent	pcDNA3.1 NES-GA_{65}-GFP	This paper		Described in Results part 1 and Materials and methods section
Recombinant DNA reagent	pcDNA3.1 NLS-GA_{65}-GFP	This paper		Described in Results part 1 and Materials and methods section
Recombinant DNA reagent	pcDNA3.1 NLS-GA_{65}-GFP (K7T, K15T)	This paper		Described in Results part 1 and Materials and methods section
Recombinant DNA reagent	pcDNA3.1 GA_{65}-GFP-PY	This paper		Described in Results part 1 and Materials and methods section
Recombinant DNA reagent	pcDNA3.1 GA_{65}-GFP-PY (P410L)	This paper		Described in Results part 1 and Materials and methods section
Recombinant DNA reagent	pcDNA3.1 GFP	This paper		Described in Results part 1 and Materials and methods section
Recombinant DNA reagent	pcDNA3.1 PR_{73}-GFP	This paper		Described in Results part 3 and Materials and methods section
Recombinant DNA reagent	pcDNA3.1 GR_{73}-GFP	This paper		Described in Results part 3 and Materials and methods section
Recombinant DNA reagent	pcDNA3.1 $(G4C2)_{73}$-GFP	This paper		Described in Results part 3 and Materials and methods section
Recombinant DNA reagent	pcDNA3.1 NLS-$(G4C2)_{73}$-GFP	This paper		Described in Results part 3 and Materials and methods section
Recombinant DNA reagent	pcDNA3.1 NES-$(G4C2)_{73}$-GFP	This paper		Described in Results part 3 and Materials and methods section
Recombinant DNA reagent	Plasmid expressing NLS-LS	PMID:31296649		Prof. F. Ulrich Hartl (Max Planck Institute for Biochemistry)
Recombinant DNA reagent	Plasmid expressing S-mApple	This paper		Described in Results part 2 and Materials and methods section
Recombinant DNA reagent	Plasmid expressing c-myc-NES-β17	PMID:26634439		Prof. F. Ulrich Hartl (Max Planck Institute for Biochemistry)
Recombinant DNA reagent	Plasmid expressing c-myc-NLS-β17	PMID:26634439		Prof. F. Ulrich Hartl (Max Planck Institute for Biochemistry)
Recombinant DNA reagent	Plasmid expressing Htt96Q	PMID:26634439		Prof. F. Ulrich Hartl (Max Planck Institute for Biochemistry)

Continued on next page

Continued

Reagent type (species) or resource	Designation	Source or reference	Identifiers	Additional information
Antibody	Mouse monoclonal anti-nuclear pore complex proteins	Abcam	Cat. #: ab24609 RRID:AB_448181	IF (1:1000)
Antibody	Mouse monoclonal anti-NPM1	Invitrogen	Cat. #: 32-5200 RRID:AB_2533084	IF (1:1000)
Antibody	Rabbit monoclonal anti-NF-κB p65 (D14E12)	Cell Signaling Technology	Cat. #: 8242 RRID:AB_10859369	IF (1:1000)
Antibody	Mouse monoclonal anti-p62	Abcam	Cat. #: ab203430 RRID:AB_2728795	IF (1:1000)
Antibody	Mouse monoclonal anti-c-Myc-Cy3 (9E10)	Sigma	Cat. #: C6594 RRID:AB_258958	IF (1:1000)
Antibody	Rabbit polyclonal anti-amyloid fibrils OC	Millipore	Cat. #: AB2286 RRID:AB_1977024	IF (1:500)
Antibody	Mouse biclonal anti-GFP	Roche	Cat. #: 11814460001 RRID:AB_390913	WB (1:1000)
Antibody	Mouse monoclonal anti-α-tubulin	Sigma	Cat. #: T6199 RRID:AB_477583	WB (1:1000)
Antibody	Mouse monoclonal anti-RPA40	Santa Cruz	Cat. #: sc-374443 RRID:AB_10991310	IF (1:1000)
Antibody	Mouse monoclonal anti-IκBα (L35A5)	Cell Signaling Technology	Cat. #: 4814 RRID:AB_390781	WB (1:/1000)
Antibody	Rabbit monoclonal anti-phospho-NF-κB p65 (Ser533) (93H1)	Cell Signaling Technology	Cat. #: 3033 RRID:AB_331284	WB (1:1000)
Antibody	Rabbit polyclonal anti-KPNA2	Abcam	Cat. #: ab70160 RRID:AB_2133673	IF (1:1000)
Antibody	Rabbit polyclonal anti-KPNA4	Abcam	Cat. #: ab84735 RRID:AB_1860702	IF (1:1000)
Antibody	Mouse monoclonal anti-KPNB1	Abcam	Cat. #: ab2811 RRID:AB_2133989	IF (1:1000)
Antibody	Mouse monoclonal anti-GAPDH	Millipore	Cat. #: MAB374 RRID:AB_2107445	WB (1:2000)
Antibody	Rabbit polyclonal anti-poly-PR	Proteintech	Cat. #: 23979-1-AP RRID:AB_2879388	WB (1:1000)
Antibody	Mouse monoclonal anti-poly-GR (5A2)	Millipore	Cat. #: MABN778 RRID:AB_2728664	WB (1:1000)
Antibody	Goat Secondary anti-mouse IgG-Alexa 488	Cell Signaling Technology	Cat. #: 4408 RRID:AB_10694704	IF (1:1000)

Continued on next page

Continued

Reagent type (species) or resource	Designation	Source or reference	Identifiers	Additional information
Antibody	Goat Secondary anti-mouse IgG-Alexa 555	Cell Signaling Technology	Cat. #: 4409 RRID:AB_1904022	IF (1:1000)
Antibody	Goat Secondary anti-rabbit IgG-Alexa 555	Cell Signaling Technology	Cat. #: 4413 RRID:AB_10694110	IF (1:1000)
Antibody	Secondary chicken anti-mouse IgG-Alexa 488	Invitrogen	Cat. #: 21200 RRID:AB_2535786	IF (1:1000)
Antibody	Secondary goat anti-mouse IgG-Alexa 633	Invitrogen	Cat. #: A21053 RRID:AB_2535720	IF (1:1000)
Antibody	Secondary goat anti-mouse IgG-peroxidase	Sigma-Aldrich	Cat. #: A4416 RRID:AB_258167	WB (1:10,000)
Antibody	Secondary goat anti-rabbit IgG-peroxidase	Sigma-Aldrich	Cat. #: A9169 RRID:AB_258434	WB (1:10,000)
Sequence-based reagent	T_{30}	PMID:26634439	FISH probe	Cy5-conjugated
Sequence-based reagent	$(C_4G_2)_5$	This paper	FISH probe	Cy3-conjugated
Chemical compound, drug	UltraPure SSC buffer	Thermo Fisher Scientific	Cat. #: 15557044	For FISH
Chemical compound, drug	Formamide	Sigma-Aldrich	Cat. #: 47671	For FISH
Chemical compound, drug	Dextran sulphate	Sigma-Aldrich	Cat. #: D6001	For FISH
Chemical compound, drug	AmyTracker 680 (AmyT)	Ebba Biotech AB	Cat. #: AmyTracker 680	Amyloid dye
Chemical compound, drug	DAPI	Invitrogen	Cat. #: D1306 RRID:AB_2629482	Nuclear stain
Chemical compound, drug	Thiazolyl blue tetrazolium bromide	Sigma Aldrich	Cat. #: M2128	For cell viability
Chemical compound, drug	N,N-dimethylformamide	Sigma-Aldrich	Cat. #: D4551	For cell viability
Chemical compound, drug	SDS	Sigma-Aldrich	Cat. #: L3771	For cell viability
Chemical compound, drug	Acetic acid	Sigma-Aldrich	Cat. #: A6283	For cell viability
Chemical compound, drug	Leptomycin B	Sigma Aldrich	Cat. #: L2913	See Materials and methods section
Commercial assay or kit	CellTiter-Glo 2.0	Promega	Cat. #: G9241	For cell viability

Continued on next page

Continued

Reagent type (species) or resource	Designation	Source or reference	Identifiers	Additional information
Commercial assay or kit	Lipofectamine 2000 transfection reagent	Thermo Fischer Scientific	Cat. #: 11668019	
Commercial assay or kit	Click-iT Plus OPP Alexa Fluor 594 Protein Synthesis Assay Kit	Thermo Fischer Scientific	Cat. #: C10457	
Peptide, recombinant protein	Human recombinant TNFα	Jena Biosciences	Cat. #: PR-430	

Cell culture, transfection, and cell treatments

Human embryonic kidney cells (ATCC-CRL-1573) were obtained from ATCC and maintained in Dulbecco's modified Eagle's medium (DMEM) (Biochrom KG) supplemented with 10% fetal bovine serum (Gibco), 100 U/ml penicillin and 100 µg/ml streptomycin sulfate (Gibco), 2 mM L-glutamine (Gibco), and 5 µg/ml Plasmocin (InvivoGen). Cells were authenticated by DNA fingerprint STR analysis by the supplier and were visually inspected using DAPI DNA staining and tested negative for mycoplasma contamination. For heat stress (HS) and recovery experiments, cells were either maintained at 37˚C (-HS), or placed in a 43˚C (+HS) incubator for the indicated duration, or subjected to heat stress and then transferred back to 37˚C for recovery (+HS + Rec). Transient transfections were performed by electroporation with the GenePulser XCell System (Bio-Rad) or with Lipofectamine 2000 (Invitrogen) according to the manufacturer's instructions. For assessing nuclear import of p65, transfected cells were treated with 20 ng/ml recombinant human TNFα (Jena Biosciences) for 30 min. For translation inhibition, cycloheximide (CHX, Sigma-Aldrich) was dissolved in phosphate buffered saline (PBS) and applied at a final concentration of 1 mM.

Plasmids

Degenerated sequences encoding 65 GA^{ggxgcx} repeats preceded by a start codon (ATG) and flanked by NheI and BamHI restriction sites were chemically synthesized by GeneArt Gene Synthesis (Invitrogen). The GC content of sequence 1 is 77.2%, while sequence 2 contains 81.5% GC (***Figure 1—figure supplement 1A***). Both GA_{65} sequences were cloned into pcDNA3.1-myc/His A plasmids in frame with GFP at the C-terminus. An N-terminal nuclear export signal (NES) or an N-terminal double SV40 nuclear localization signal (NLS) was inserted by site-directed mutagenesis. The alternative FUS-derived nuclear localization signal (PY) was inserted C-terminally. Point mutations were introduced by site-directed mutagenesis. Similarly, degenerated sequences encoding PR_{73} and GR_{73} were generated by GeneArt Gene Synthesis (Invitrogen) and fused to the N-terminus of GFP. All sequences contained an ATG start codon. Sequences encoding $(G_4C_2)_{73}$ repeats preceded by a start codon (ATG) were generated as previously described by primer hybridization (***Guo et al., 2018***). Similarly, the $(G_4C_2)_{73}$ construct was subcloned in place of the degenerated GA_{65} sequence in the same NES/NLS-tagged GFP-containing vector. A GFP-only construct was generated by deletion of the GA from the same vector. NLS-LS has been previously described (***Frottin et al., 2019***). The plasmid encoding for S-mApple was generated from mApple-N1 (Addgene plasmid # 54567), a kind gift from Michael Davidson (***Shaner et al., 2008***). mApple was then cloned between BamHI and XbaI to replace GFP in a previously described plasmid encoding shuttle GFP (***Woerner et al., 2016***). c-myc-NES-β17, c-myc-NLS-β17, and Htt96Q plasmids have been previously described (***Woerner et al., 2016***). All relevant plasmid regions were verified by sequencing.

Antibodies and dyes

The following primary antibodies were used in this study: nuclear pore complex proteins (Mab414), Abcam (24609); NPM1, Invitrogen (32-5200); NF-κB p65 (D14E12), Cell Signaling Technology (#8242); c-Myc-Cy3 (9E10), Sigma (C6594); amyloid fibrils, OC, Millipore (AB2286); GFP, Roche (11814460001); α-tubulin, Sigma Aldrich (T6199); RPA40, Santa Cruz (sc-374443); IκBα (L35A5), Cell Signaling Technology (#4814); phospho-NF-κB p65 (Ser536) (93H1), Cell Signaling Technology

(#3033); KPNA2, Abcam (ab70160); KPNA4, Abcam (ab84735); KPNB1, Abcam (ab2811); GAPDH, Millipore (MAB374); poly-PR, Proteintech (23979-1-AP); and poly-GR (5A2), Millipore (MABN778).

The following secondary antibodies were used: mouse IgG-Alexa488, Cell Signaling Technology (#4408); mouse IgG-Alexa555, Cell Signaling Technology (#4409); rabbit IgG-Alexa555, Cell Signaling Technology (#4413); mouse IgG-Alexa488, Invitrogen (21200); mouse IgG-Alexa 633, Invitrogen (A21053); anti-mouse IgG-Peroxidase, Sigma Aldrich (A4416); and anti-rabbit IgG-Peroxidase, Sigma Aldrich (A9169). The amyloid dye AmyTracker 680 (AmyT; Ebba Biotech AB) was used as previously described (***Frottin et al., 2019***). Briefly, cells were fixed in 4% paraformaldehyde in PBS (Gibco) for 20 min, washed with PBS, and permeabilized with Triton X-100 0.1% for 5 min. AmyT was used at 1:500 dilution and incubated with the samples for 1 hr at room temperature. Nuclei were counterstained with 4',6-diamidine-2'-phenylindole dihydrochloride (DAPI, Molecular Probes).

Immunofluorescence and image acquisition

Cells were grown on poly-L-lysine-coated coverslips (Neuvitro). Cells were fixed with 4% paraformaldehyde, permeabilized with 0.1% Triton X-100, and blocked with 1% bovine serum albumin in PBS. Primary antibodies were applied in blocking buffer supplemented with 0.1% Triton X-100 and incubated overnight at 4˚C. Appropriate fluorescent secondary antibodies at a dilution of 1:500 were applied for 60 min at room temperature. Nuclei were counterstained with DAPI before mounting samples with fluorescence-compatible mounting medium (DAKO).

Confocal microscopy was performed at MPIB Imaging Facility (Martinsried, Germany) on a ZEISS (Jena, Germany) LSM780 confocal laser scanning microscope equipped with a ZEISS Plan-APO 63×/NA1.46 oil immersion objective. In case of multi-fluorescence samples, a single-stained control sample was used to adjust emission and detection configuration to minimize spectral bleed-through. Images of cells with inclusions for co-localization studies were subjected to linear unmixing with spectra obtained from the single-stained samples using ZEN software. When fluorescence intensities were directly compared, acquisition settings and processing were kept identical. Images were analyzed with ImageJ (Rasband, W.S., National Institutes of Health, USA) and assembled in Adobe Photoshop CC (Adobe Systems Incorporated, Release 19.1.5).

Cell viability assay

HEK293 cells were transfected by electroporation as previously described (***Woerner et al., 2016***). In brief, cells were electroporated with 20 µg of plasmid in 0.4 cm-gap electroporation cuvettes (Bio-Rad). Cells were electroporated at 225 V, ∞ Ω, 950 µF exponential wave in a GenePulser XCell System (Bio-Rad). After electroporation, cells were plated in a 24-well plate in triplicates. MTT assays were performed 3 days after transfection. The growth medium was replaced with fresh medium containing 5 µg/ml thiazolyl blue tetrazolium bromide (Sigma) for 1 hr. Formazan crystals were solubilized by addition of stop solution, containing 40% N,N-dimethylformamide (Sigma-Aldrich), 16% SDS (Sigma-Aldrich), and 2% (v/v) acetic acid (Sigma-Aldrich). Absorbance at 570 nm and 630 nm was then recorded. Alternatively, viability was measured using the CellTiter-Glo 2.0 Cell Viability Assay kit (Promega) in the same conditions.

Determination of nuclear import/export with S-mApple

Cells were co-transfected with the indicated constructs and the reporter S-mApple. After 48 hr, cells were treated with 10 ng/ml of the CRM1 inhibitor Leptomycin B (LMB, Sigma Aldrich) in DMSO for 15 min before cell fixation. Control cells received DMSO. The relative concentration of S-mApple in the cytoplasm and nucleus was quantified by measuring the fluorescence intensity ratio in cells from three independent experiments. Fluorescence intensities were determined using ImageJ.

Protein biosynthesis assay by click-chemistry

Protein biosynthesis assays were carried out using the click-it plus O-propargyl-puromycin (OPP) protein synthesis assay (Thermo Fisher Scientific) according to the manufacturer's instructions. Cells were transfected for 24 hr with the indicated construct before metabolic labeling and incubated with the OPP reagent for 30 min in normal growth conditions. As control, protein translation was inhibited with cycloheximide (CHX, Sigma-Aldrich) dissolved in PBS and applied at a final concentration of 1 mM. Samples were then fixed, permeabilized, and the click reaction performed as

recommended by the provider. Samples were subsequently analyzed by confocal microscopy. The concentration of labeled proteins was quantified by measuring the mean fluorescence intensity in 100–250 cells using ImageJ. A representative experiment of three independent experiments is shown.

Fluorescence in situ hybridization (FISH)

Visualization of mRNA and G_4C_2 RNA by FISH was carried out as previously described (***Woerner et al., 2016***). HEK293 cells were fixed in 4% formaldehyde for 10 min at room temperature and permeabilized with 0.1% Triton X-100, both in UltraPure SCC buffer (Thermo Fisher Scientific). After washing with SSC buffer and with FISH buffer (10% formamide in SCC buffer), the probes (either T30 or $(C_4G_2)_5$) were hybridized in FISH buffer with 10% dextran sulphate (Sigma Aldrich) for 3 hr at 42˚C, followed by additional washes in FISH buffer. When required, immunostaining was performed in PBS-based buffers afterward. The fraction of transfected cells displaying abnormal accumulation of mRNA (using poly-dT probe) within the nucleus was determined by confocal microscopy.

Filter retardation assay

For the filter retardation assay (***Scherzinger et al., 1997***; ***Wanker et al., 1999***), cells were harvested 24 hr after transfection with the indicated plasmids, lysed in radioimmunoprecipitation assay (RIPA) buffer (Thermo Fisher Scientific) and sonicated for 10 s. After incubation for 30 min, protein concentration was measured by Bradford assay (Bio-Rad), and equal amounts of lysates were filtered through a 0.2 µm pore size cellulose acetate membrane (GE Healthcare) and washed with lysis buffer. The membrane was subsequently immunoassayed with anti-GFP antibody. Antibody binding was detected using Luminata Forte Western HRP substrate (Millipore), and pictures were acquired with a LAS-3000 camera system (Fujifilm). AIDA (Raytest) software was used for analysis and quantitation.

Statistics

Significance of differences between samples was determined using unpaired Student's t-test, unless stated otherwise. Significance levels: *p<0.05, **p<0.01, ***p<0.001.

Acknowledgements

We thank R Klein, D Edbauer, R Körner, and R Sawarkar for helpful discussions. We acknowledge technical support by the MPIB Imaging facility. Funding: The research leading to these results has received funding from the European Commission under grant FP7 GA ERC-2012-SyG_318987–ToPAG. FF was supported by an EMBO Long Term Fellowship. MPB was supported by the Lehre@LMU Student Research Award Program of the Faculty of Biology at LMU Munich (sponsored by the Federal Ministry of Education and Research, funding no. 01PL17016).

Additional information

Competing interests

F Ulrich Hartl: Reviewing editor, *eLife*. The other authors declare that no competing interests exist.

Funding

Funder	Grant reference number	Author
EMBO	Long term fellowship	Frédéric Frottin
European Commission	FP7 GA ERC-2012-SyG_318987-ToPAG	F Ulrich Hartl
Federal Ministry of Education and Research	01PL17016	Manuela Pérez-Berlanga
Max Planck Society		Mark S Hipp

The funders had no role in study design, data collection and interpretation, or the decision to submit the work for publication.

Author contributions

Frédéric Frottin, Conceptualization, Supervision, Investigation, Writing - original draft, Writing - review and editing; Manuela Pérez-Berlanga, Investigation, Writing - review and editing; F Ulrich Hartl, Mark S Hipp, Conceptualization, Supervision, Writing - original draft, Writing - review and editing

Author ORCIDs

Frédéric Frottin https://orcid.org/0000-0002-2756-7838
Manuela Pérez-Berlanga http://orcid.org/0000-0001-9064-9724
F Ulrich Hartl https://orcid.org/0000-0002-7941-135X
Mark S Hipp https://orcid.org/0000-0002-0497-3016

Decision letter and Author response

Decision letter https://doi.org/10.7554/eLife.62718.sa1
Author response https://doi.org/10.7554/eLife.62718.sa2

Additional files

Supplementary files

- Transparent reporting form

Data availability

All data generated or analysed during this study are included in the manuscript and supporting files.

References

Al-Sarraj S, King A, Troakes C, Smith B, Maekawa S, Bodi I, Rogelj B, Al-Chalabi A, Hortobágyi T, Shaw CE. 2011. p62 positive, TDP-43 negative, neuronal cytoplasmic and intranuclear inclusions in the cerebellum and Hippocampus define the pathology of C9orf72-linked FTLD and MND/ALS. *Acta Neuropathologica* **122**:691–702. DOI: https://doi.org/10.1007/s00401-011-0911-2, PMID: 22101323

Almeida S, Gascon E, Tran H, Chou HJ, Gendron TF, Degroot S, Tapper AR, Sellier C, Charlet-Berguerand N, Karydas A, Seeley WW, Boxer AL, Petrucelli L, Miller BL, Gao FB. 2013. Modeling key pathological features of frontotemporal dementia with C9ORF72 repeat expansion in iPSC-derived human neurons. *Acta Neuropathologica* **126**:385–399. DOI: https://doi.org/10.1007/s00401-013-1149-y, PMID: 23836290

Arzberger T, Schludi MH, Lehmer C, Schmid B, Edbauer D. 2018. RNA versus protein toxicity in C9orf72 ALS/FTLD. *Acta Neuropathologica* **135**:475–479. DOI: https://doi.org/10.1007/s00401-018-1823-1, PMID: 29450647

Ash PE, Bieniek KF, Gendron TF, Caulfield T, Lin WL, Dejesus-Hernandez M, van Blitterswijk MM, Jansen-West K, Paul JW, Rademakers R, Boylan KB, Dickson DW, Petrucelli L. 2013. Unconventional translation of C9ORF72 GGGGCC expansion generates insoluble polypeptides specific to c9FTD/ALS. *Neuron* **77**:639–646. DOI: https://doi.org/10.1016/j.neuron.2013.02.004, PMID: 23415312

Atanasio A, Decman V, White D, Ramos M, Ikiz B, Lee HC, Siao CJ, Brydges S, LaRosa E, Bai Y, Fury W, Burfeind P, Zamfirova R, Warshaw G, Orengo J, Oyejide A, Fralish M, Auerbach W, Poueymirou W, Freudenberg J, et al. 2016. C9orf72 ablation causes immune dysregulation characterized by leukocyte expansion, autoantibody production, and glomerulonephropathy in mice. *Scientific Reports* **6**:23204. DOI: https://doi.org/10.1038/srep23204, PMID: 26979938

Balendra R, Isaacs AM. 2018. C9orf72-mediated ALS and FTD: multiple pathways to disease. *Nature Reviews Neurology* **14**:544–558. DOI: https://doi.org/10.1038/s41582-018-0047-2, PMID: 30120348

Boeynaems S, Bogaert E, Michiels E, Gijselinck I, Sieben A, Jovičić A, De Baets G, Scheveneels W, Steyaert J, Cuijt I, Verstrepen KJ, Callaerts P, Rousseau F, Schymkowitz J, Cruts M, Van Broeckhoven C, Van Damme P, Gitler AD, Robberecht W, Van Den Bosch L. 2016. *Drosophila* screen connects nuclear transport genes to DPR pathology in c9ALS/FTD. *Scientific Reports* **6**:20877. DOI: https://doi.org/10.1038/srep20877, PMID: 26869068

Boeynaems S, Bogaert E, Kovacs D, Konijnenberg A, Timmerman E, Volkov A, Guharoy M, De Decker M, Jaspers T, Ryan VH, Janke AM, Baatsen P, Vercruysse T, Kolaitis R-M, Daelemans D, Taylor JP, Kedersha N, Anderson P, Impens F, Sobott F, et al. 2017. Phase separation of C9orf72 dipeptide repeats perturbs stress granule dynamics. *Molecular Cell* **65**:1044–1055. DOI: https://doi.org/10.1016/j.molcel.2017.02.013

Boivin M, Pfister V, Gaucherot A, Ruffenach F, Negroni L, Sellier C, Charlet-Berguerand N. 2020. Reduced autophagy upon C9ORF72 loss synergizes with dipeptide repeat protein toxicity in G4C2 repeat expansion disorders. *The EMBO Journal* **39**:e100574. DOI: https://doi.org/10.15252/embj.2018100574, PMID: 31930538

Burberry A, Suzuki N, Wang JY, Moccia R, Mordes DA, Stewart MH, Suzuki-Uematsu S, Ghosh S, Singh A, Merkle FT, Koszka K, Li QZ, Zon L, Rossi DJ, Trowbridge JJ, Notarangelo LD, Eggan K. 2016. Loss-of-function mutations in the *C9ORF72* mouse ortholog cause fatal autoimmune disease. *Science Translational Medicine* **8**: 347ra93. DOI: https://doi.org/10.1126/scitranslmed.aaf6038, PMID: 27412785

Burberry A, Wells MF, Limone F, Couto A, Smith KS, Keaney J, Gillet G, van Gastel N, Wang JY, Pietilainen O, Qian M, Eggan P, Cantrell C, Mok J, Kadiu I, Scadden DT, Eggan K. 2020. C9orf72 suppresses systemic and neural inflammation induced by gut Bacteria. *Nature* **582**:89–94. DOI: https://doi.org/10.1038/s41586-020-2288-7, PMID: 32483373

Carter KC, Taneja KL, Lawrence JB. 1991. Discrete nuclear domains of poly(A) RNA and their relationship to the functional organization of the nucleus. *The Journal of Cell Biology* **115**:1191–1202. DOI: https://doi.org/10.1083/jcb.115.5.1191, PMID: 1720123

Chou CC, Zhang Y, Umoh ME, Vaughan SW, Lorenzini I, Liu F, Sayegh M, Donlin-Asp PG, Chen YH, Duong DM, Seyfried NT, Powers MA, Kukar T, Hales CM, Gearing M, Cairns NJ, Boylan KB, Dickson DW, Rademakers R, Zhang YJ, et al. 2018. TDP-43 pathology disrupts nuclear pore complexes and nucleocytoplasmic transport in ALS/FTD. *Nature Neuroscience* **21**:228–239. DOI: https://doi.org/10.1038/s41593-017-0047-3, PMID: 29311743

Cook CN, Wu Y, Odeh HM, Gendron TF, Jansen-West K, Del Rosso G, Yue M, Jiang P, Gomes E, Tong J, Daughrity LM, Avendano NM, Castanedes-Casey M, Shao W, Oskarsson B, Tomassy GS, McCampbell A, Rigo F, Dickson DW, Shorter J, et al. 2020. *C9orf72* poly(GR) aggregation induces TDP-43 proteinopathy. *Science Translational Medicine* **12**:eabb3774. DOI: https://doi.org/10.1126/scitranslmed.abb3774, PMID: 32878979

Cooper-Knock J, Walsh MJ, Higginbottom A, Robin Highley J, Dickman MJ, Edbauer D, Ince PG, Wharton SB, Wilson SA, Kirby J, Hautbergue GM, Shaw PJ. 2014. Sequestration of multiple RNA recognition motif-containing proteins by C9orf72 repeat expansions. *Brain* **137**:2040–2051. DOI: https://doi.org/10.1093/brain/awu120, PMID: 24866055

Cooper-Knock J, Higginbottom A, Stopford MJ, Highley JR, Ince PG, Wharton SB, Pickering-Brown S, Kirby J, Hautbergue GM, Shaw PJ. 2015. Antisense RNA foci in the motor neurons of C9ORF72-ALS patients are associated with TDP-43 proteinopathy. *Acta Neuropathologica* **130**:63–75. DOI: https://doi.org/10.1007/s00401-015-1429-9, PMID: 25943887

Davidson Y, Robinson AC, Liu X, Wu D, Troakes C, Rollinson S, Masuda-Suzukake M, Suzuki G, Nonaka T, Shi J, Tian J, Hamdalla H, Ealing J, Richardson A, Jones M, Pickering-Brown S, Snowden JS, Hasegawa M, Mann DM. 2016. Neurodegeneration in frontotemporal lobar degeneration and motor neurone disease associated with expansions in C9orf72 is linked to TDP-43 pathology and not associated with aggregated forms of dipeptide repeat proteins. *Neuropathology and Applied Neurobiology* **42**:242–254. DOI: https://doi.org/10.1111/nan.12292, PMID: 26538301

DeJesus-Hernandez M, Mackenzie IR, Boeve BF, Boxer AL, Baker M, Rutherford NJ, Nicholson AM, Finch NA, Flynn H, Adamson J, Kouri N, Wojtas A, Sengdy P, Hsiung GY, Karydas A, Seeley WW, Josephs KA, Coppola G, Geschwind DH, Wszolek ZK, et al. 2011. Expanded GGGGCC hexanucleotide repeat in noncoding region of C9ORF72 causes chromosome 9p-linked FTD and ALS. *Neuron* **72**:245–256. DOI: https://doi.org/10.1016/j.neuron.2011.09.011, PMID: 21944778

Donnelly CJ, Zhang PW, Pham JT, Haeusler AR, Heusler AR, Mistry NA, Vidensky S, Daley EL, Poth EM, Hoover B, Fines DM, Maragakis N, Tienari PJ, Petrucelli L, Traynor BJ, Wang J, Rigo F, Bennett CF, Blackshaw S, Sattler R, et al. 2013. RNA toxicity from the ALS/FTD C9ORF72 expansion is mitigated by antisense intervention. *Neuron* **80**:415–428. DOI: https://doi.org/10.1016/j.neuron.2013.10.015, PMID: 24139042

Dormann D, Rodde R, Edbauer D, Bentmann E, Fischer I, Hruscha A, Than ME, Mackenzie IR, Capell A, Schmid B, Neumann M, Haass C. 2010. ALS-associated fused in sarcoma (FUS) mutations disrupt Transportin-mediated nuclear import. *The EMBO Journal* **29**:2841–2857. DOI: https://doi.org/10.1038/emboj.2010.143, PMID: 20606625

Eftekharzadeh B, Daigle JG, Kapinos LE, Coyne A, Schiantarelli J, Carlomagno Y, Cook C, Miller SJ, Dujardin S, Amaral AS, Grima JC, Bennett RE, Tepper K, DeTure M, Vanderburg CR, Corjuc BT, DeVos SL, Gonzalez JA, Chew J, Vidensky S, et al. 2019. Tau protein disrupts nucleocytoplasmic transport in Alzheimer's Disease. *Neuron* **101**:349. DOI: https://doi.org/10.1016/j.neuron.2018.12.031, PMID: 30653936

Freibaum BD, Lu Y, Lopez-Gonzalez R, Kim NC, Almeida S, Lee KH, Badders N, Valentine M, Miller BL, Wong PC, Petrucelli L, Kim HJ, Gao FB, Taylor JP. 2015. GGGGCC repeat expansion in C9orf72 compromises nucleocytoplasmic transport. *Nature* **525**:129–133. DOI: https://doi.org/10.1038/nature14974, PMID: 26308899

Frottin F, Schueder F, Tiwary S, Gupta R, Körner R, Schlichthaerle T, Cox J, Jungmann R, Hartl FU, Hipp MS. 2019. The nucleolus functions as a phase-separated protein quality control compartment. *Science* **365**:342–347. DOI: https://doi.org/10.1126/science.aaw9157, PMID: 31296649

Gal J, Zhang J, Kwinter DM, Zhai J, Jia H, Jia J, Zhu H. 2011. Nuclear localization sequence of FUS and induction of stress granules by ALS mutants. *Neurobiology of Aging* **32**:2323.e27. DOI: https://doi.org/10.1016/j.neurobiolaging.2010.06.010

Gasset-Rosa F, Chillon-Marinas C, Goginashvili A, Atwal RS, Artates JW, Tabet R, Wheeler VC, Bang AG, Cleveland DW, Lagier-Tourenne C. 2017. Polyglutamine-Expanded huntingtin exacerbates Age-Related disruption of nuclear integrity and nucleocytoplasmic transport. *Neuron* **94**:48–57. DOI: https://doi.org/10.1016/j.neuron.2017.03.027

Gendron TF, Bieniek KF, Zhang YJ, Jansen-West K, Ash PE, Caulfield T, Daughrity L, Dunmore JH, Castanedes-Casey M, Chew J, Cosio DM, van Blitterswijk M, Lee WC, Rademakers R, Boylan KB, Dickson DW, Petrucelli L. 2013. Antisense transcripts of the expanded C9ORF72 hexanucleotide repeat form nuclear RNA foci and undergo repeat-associated non-ATG translation in c9FTD/ALS. *Acta Neuropathologica* **126**:829–844. DOI: https://doi.org/10.1007/s00401-013-1192-8, PMID: 24129584

Gijselinck I, Van Mossevelde S, van der Zee J, Sieben A, Engelborghs S, De Bleecker J, Ivanoiu A, Deryck O, Edbauer D, Zhang M, Heeman B, Bäumer V, Van den Broeck M, Mattheijssens M, Peeters K, Rogaeva E, De Jonghe P, Cras P, Martin JJ, de Deyn PP, et al. 2016. The C9orf72 repeat size correlates with onset age of disease, DNA methylation and transcriptional downregulation of the promoter. *Molecular Psychiatry* **21**:1112–1124. DOI: https://doi.org/10.1038/mp.2015.159, PMID: 26481318

Gitler AD, Tsuiji H. 2016. There has been an awakening: emerging mechanisms of C9orf72 mutations in FTD/ALS. *Brain Research* **1647**:19–29. DOI: https://doi.org/10.1016/j.brainres.2016.04.004, PMID: 27059391

Grima JC, Daigle JG, Arbez N, Cunningham KC, Zhang K, Ochaba J, Geater C, Morozko E, Stocksdale J, Glatzer JC, Pham JT, Ahmed I, Peng Q, Wadhwa H, Pletnikova O, Troncoso JC, Duan W, Snyder SH, Ranum LPW, Thompson LM, et al. 2017. Mutant huntingtin disrupts the nuclear pore complex. *Neuron* **94**:93–107. DOI: https://doi.org/10.1016/j.neuron.2017.03.023

Guo Q, Lehmer C, Martínez-Sánchez A, Rudack T, Beck F, Hartmann H, Pérez-Berlanga M, Frottin F, Hipp MS, Hartl FU, Edbauer D, Baumeister W, Fernández-Busnadiego R. 2018. In situ structure of neuronal C9orf72 Poly-GA aggregates reveals proteasome recruitment. *Cell* **172**:696–705. DOI: https://doi.org/10.1016/j.cell.2017.12.030, PMID: 29398115

Haeusler AR, Donnelly CJ, Periz G, Simko EA, Shaw PG, Kim MS, Maragakis NJ, Troncoso JC, Pandey A, Sattler R, Rothstein JD, Wang J. 2014. C9orf72 nucleotide repeat structures initiate molecular cascades of disease. *Nature* **507**:195–200. DOI: https://doi.org/10.1038/nature13124, PMID: 24598541

Hayes LR, Duan L, Bowen K, Kalab P, Rothstein JD. 2020. *C9orf72* arginine-rich dipeptide repeat proteins disrupt karyopherin-mediated nuclear import. *eLife* **9**:e51685. DOI: https://doi.org/10.7554/eLife.51685, PMID: 32119645

Jiang J, Zhu Q, Gendron TF, Saberi S, McAlonis-Downes M, Seelman A, Stauffer JE, Jafar-Nejad P, Drenner K, Schulte D, Chun S, Sun S, Ling SC, Myers B, Engelhardt J, Katz M, Baughn M, Platoshyn O, Marsala M, Watt A, et al. 2016. Gain of toxicity from ALS/FTD-Linked repeat expansions in C9ORF72 is alleviated by antisense oligonucleotides targeting GGGGCC-Containing RNAs. *Neuron* **90**:535–550. DOI: https://doi.org/10.1016/j.neuron.2016.04.006, PMID: 27112497

Jiang J, Ravits J. 2019. Pathogenic mechanisms and therapy development for C9orf72 amyotrophic lateral sclerosis/Frontotemporal dementia. *Neurotherapeutics* **16**:1115–1132. DOI: https://doi.org/10.1007/s13311-019-00797-2, PMID: 31667754

Jovičić A, Mertens J, Boeynaems S, Bogaert E, Chai N, Yamada SB, Paul JW, Sun S, Herdy JR, Bieri G, Kramer NJ, Gage FH, Van Den Bosch L, Robberecht W, Gitler AD. 2015. Modifiers of C9orf72 dipeptide repeat toxicity connect nucleocytoplasmic transport defects to FTD/ALS. *Nature Neuroscience* **18**:1226–1229. DOI: https://doi.org/10.1038/nn.4085, PMID: 26308983

Kanekura K, Yagi T, Cammack AJ, Mahadevan J, Kuroda M, Harms MB, Miller TM, Urano F. 2016. Poly-dipeptides encoded by the C9ORF72 repeats block global protein translation. *Human Molecular Genetics* **25**:1803–1813. DOI: https://doi.org/10.1093/hmg/ddw052, PMID: 26931465

Kayed R, Head E, Sarsoza F, Saing T, Cotman CW, Necula M, Margol L, Wu J, Breydo L, Thompson JL, Rasool S, Gurlo T, Butler P, Glabe CG. 2007. Fibril specific, conformation dependent antibodies recognize a generic epitope common to amyloid fibrils and fibrillar oligomers that is absent in prefibrillar oligomers. *Molecular Neurodegeneration* **2**:18. DOI: https://doi.org/10.1186/1750-1326-2-18, PMID: 17897471

Khosravi B, Hartmann H, May S, Möhl C, Ederle H, Michaelsen M, Schludi MH, Dormann D, Edbauer D. 2017. Feb 15). Cytoplasmic poly-GA aggregates impair nuclear import of TDP-43 in C9orf72 ALS/FTLD. *Human Molecular Genetics* **26**:790–800. DOI: https://doi.org/10.1093/hmg/ddw432, PMID: 28040728

Khosravi B, LaClair KD, Riemenschneider H, Zhou Q, Frottin F, Mareljic N, Czuppa M, Farny D, Hartmann H, Michaelsen M, Arzberger T, Hartl FU, Hipp MS, Edbauer D. 2020. Cell-to-cell transmission of C9orf72 poly-(Gly-Ala) triggers key features of ALS/FTD. *The EMBO Journal* **39**:e102811. DOI: https://doi.org/10.15252/embj.2019102811, PMID: 32175624

Koppers M, Blokhuis AM, Westeneng HJ, Terpstra ML, Zundel CA, Vieira de Sá R, Schellevis RD, Waite AJ, Blake DJ, Veldink JH, van den Berg LH, Pasterkamp RJ. 2015. C9orf72 ablation in mice does not cause motor neuron degeneration or motor deficits. *Annals of Neurology* **78**:426–438. DOI: https://doi.org/10.1002/ana.24453, PMID: 26044557

Kramer NJ, Haney MS, Morgens DW, Jovičić A, Couthouis J, Li A, Ousey J, Ma R, Bieri G, Tsui CK, Shi Y, Hertz NT, Tessier-Lavigne M, Ichida JK, Bassik MC, Gitler AD. 2018. CRISPR-Cas9 screens in human cells and primary neurons identify modifiers of C9ORF72 dipeptide-repeat-protein toxicity. *Nature Genetics* **50**:603–612. DOI: https://doi.org/10.1038/s41588-018-0070-7, PMID: 29507424

Kwon I, Xiang S, Kato M, Wu L, Theodoropoulos P, Wang T, Kim J, Yun J, Xie Y, McKnight SL. 2014. Poly-dipeptides encoded by the C9orf72 repeats bind nucleoli, impede RNA biogenesis, and kill cells. *Science* **345**:1139–1145. DOI: https://doi.org/10.1126/science.1254917, PMID: 25081482

Lagier-Tourenne C, Baughn M, Rigo F, Sun S, Liu P, Li HR, Jiang J, Watt AT, Chun S, Katz M, Qiu J, Sun Y, Ling SC, Zhu Q, Polymenidou M, Drenner K, Artates JW, McAlonis-Downes M, Markmiller S, Hutt KR, et al. 2013. Targeted degradation of sense and antisense C9orf72 RNA foci as therapy for ALS and frontotemporal degeneration. *PNAS* **110**:E4530–E4539. DOI: https://doi.org/10.1073/pnas.1318835110, PMID: 24170860

Lee K-H, Zhang P, Kim HJ, Mitrea DM, Sarkar M, Freibaum BD, Cika J, Coughlin M, Messing J, Molliex A, Maxwell BA, Kim NC, Temirov J, Moore J, Kolaitis R-M, Shaw TI, Bai B, Peng J, Kriwacki RW, Taylor JP. 2016. C9orf72 dipeptide repeats impair the assembly, dynamics, and function of Membrane-Less organelles. *Cell* **167**:774–788. DOI: https://doi.org/10.1016/j.cell.2016.10.002

Lee YB, Baskaran P, Gomez-Deza J, Chen HJ, Nishimura AL, Smith BN, Troakes C, Adachi Y, Stepto A, Petrucelli L, Gallo JM, Hirth F, Rogelj B, Guthrie S, Shaw CE. 2017. C9orf72 poly GA RAN-translated protein plays a key role in amyotrophic lateral sclerosis via aggregation and toxicity. *Human Molecular Genetics* **26**:4765–4777. DOI: https://doi.org/10.1093/hmg/ddx350, PMID: 28973350

Lin Y, Mori E, Kato M, Xiang S, Wu L, Kwon I, McKnight SL. 2016. Toxic PR Poly-Dipeptides encoded by the C9orf72 repeat expansion target LC domain polymers. *Cell* **167**:789–802. DOI: https://doi.org/10.1016/j.cell.2016.10.003

Liu Y, Pattamatta A, Zu T, Reid T, Bardhi O, Borchelt DR, Yachnis AT, Ranum LP. 2016. C9orf72 BAC mouse model with motor deficits and neurodegenerative features of ALS/FTD. *Neuron* **90**:521–534. DOI: https://doi.org/10.1016/j.neuron.2016.04.005, PMID: 27112499

Mackenzie IR, Frick P, Grässer FA, Gendron TF, Petrucelli L, Cashman NR, Edbauer D, Kremmer E, Prudlo J, Troost D, Neumann M. 2015. Quantitative analysis and clinico-pathological correlations of different dipeptide repeat protein pathologies in C9ORF72 mutation carriers. *Acta Neuropathologica* **130**:845–861. DOI: https://doi.org/10.1007/s00401-015-1476-2, PMID: 26374446

May S, Hornburg D, Schludi MH, Arzberger T, Rentzsch K, Schwenk BM, Grässer FA, Mori K, Kremmer E, Banzhaf-Strathmann J, Mann M, Meissner F, Edbauer D. 2014. C9orf72 FTLD/ALS-associated Gly-Ala dipeptide repeat proteins cause neuronal toxicity and Unc119 sequestration. *Acta Neuropathologica* **128**:485–503. DOI: https://doi.org/10.1007/s00401-014-1329-4, PMID: 25120191

Mizielinska S, Ridler CE, Balendra R, Thoeng A, Woodling NS, Grässer FA, Plagnol V, Lashley T, Partridge L, Isaacs AM. 2017. Bidirectional nucleolar dysfunction in C9orf72 frontotemporal lobar degeneration. *Acta Neuropathologica Communications* **5**:29. DOI: https://doi.org/10.1186/s40478-017-0432-x, PMID: 28420437

Moens TG, Niccoli T, Wilson KM, Atilano ML, Birsa N, Gittings LM, Holbling BV, Dyson MC, Thoeng A, Neeves J, Glaria I, Yu L, Bussmann J, Storkebaum E, Pardo M, Choudhary JS, Fratta P, Partridge L, Isaacs AM. 2019. C9orf72 arginine-rich dipeptide proteins interact with ribosomal proteins in vivo to induce a toxic translational arrest that is rescued by eIF1A. *Acta Neuropathologica* **137**:487–500. DOI: https://doi.org/10.1007/s00401-018-1946-4, PMID: 30604225

Mori K, Arzberger T, Grässer FA, Gijselinck I, May S, Rentzsch K, Weng SM, Schludi MH, van der Zee J, Cruts M, Van Broeckhoven C, Kremmer E, Kretzschmar HA, Haass C, Edbauer D. 2013a. Bidirectional transcripts of the expanded C9orf72 hexanucleotide repeat are translated into aggregating dipeptide repeat proteins. *Acta Neuropathologica* **126**:881–893. DOI: https://doi.org/10.1007/s00401-013-1189-3, PMID: 24132570

Mori K, Lammich S, Mackenzie IR, Forné I, Zilow S, Kretzschmar H, Edbauer D, Janssens J, Kleinberger G, Cruts M, Herms J, Neumann M, Van Broeckhoven C, Arzberger T, Haass C. 2013b. hnRNP A3 binds to GGGGCC repeats and is a constituent of p62-positive/TDP43-negative inclusions in the Hippocampus of patients with C9orf72 mutations. *Acta Neuropathologica* **125**:413–423. DOI: https://doi.org/10.1007/s00401-013-1088-7, PMID: 23381195

Mori K, Weng SM, Arzberger T, May S, Rentzsch K, Kremmer E, Schmid B, Kretzschmar HA, Cruts M, Van Broeckhoven C, Haass C, Edbauer D. 2013c. The C9orf72 GGGGCC repeat is translated into aggregating dipeptide-repeat proteins in FTLD/ALS. *Science* **339**:1335–1338. DOI: https://doi.org/10.1126/science.1232927, PMID: 23393093

Nihei Y, Mori K, Werner G, Arzberger T, Zhou Q, Khosravi B, Japtok J, Hermann A, Sommacal A, Weber M, Kamp F, Nuscher B, Edbauer D, Haass C, German Consortium for Frontotemporal Lobar Degeneration, Bavarian Brain Banking Alliance. 2020. Poly-glycine-alanine exacerbates C9orf72 repeat expansion-mediated DNA damage via sequestration of phosphorylated ATM and loss of nuclear hnRNPA3. *Acta Neuropathologica* **139**:99–118. DOI: https://doi.org/10.1007/s00401-019-02082-0, PMID: 31642962

Nonaka T, Masuda-Suzukake M, Hosokawa M, Shimozawa A, Hirai S, Okado H, Hasegawa M. 2018. C9ORF72 dipeptide repeat poly-GA inclusions promote intracellular aggregation of phosphorylated TDP-43. *Human Molecular Genetics* **27**:2658–2670. DOI: https://doi.org/10.1093/hmg/ddy174, PMID: 29750243

Nordin A, Akimoto C, Wuolikainen A, Alstermark H, Jonsson P, Birve A, Marklund SL, Graffmo KS, Forsberg K, Brännström T, Andersen PM. 2015. Extensive size variability of the GGGGCC expansion in C9orf72 in both neuronal and non-neuronal tissues in 18 patients with ALS or FTD. *Human Molecular Genetics* **24**:3133–3142. DOI: https://doi.org/10.1093/hmg/ddv064, PMID: 25712133

O'Rourke JG, Bogdanik L, Yáñez A, Lall D, Wolf AJ, Muhammad AK, Ho R, Carmona S, Vit JP, Zarrow J, Kim KJ, Bell S, Harms MB, Miller TM, Dangler CA, Underhill DM, Goodridge HS, Lutz CM, Baloh RH. 2016. C9orf72 is required for proper macrophage and microglial function in mice. *Science* **351**:1324–1329. DOI: https://doi.org/10.1126/science.aaf1064, PMID: 26989253

Ohki Y, Wenninger-Weinzierl A, Hruscha A, Asakawa K, Kawakami K, Haass C, Edbauer D, Schmid B. 2017. Glycine-alanine dipeptide repeat protein contributes to toxicity in a zebrafish model of C9orf72 associated neurodegeneration. *Molecular Neurodegeneration* **12**:6. DOI: https://doi.org/10.1186/s13024-016-0146-8, PMID: 28088213

Panda SK, Wefers B, Ortiz O, Floss T, Schmid B, Haass C, Wurst W, Kühn R. 2013. Highly efficient targeted mutagenesis in mice using TALENs. *Genetics* **195**:703–713. DOI: https://doi.org/10.1534/genetics.113.156570, PMID: 23979585

Radwan M, Ang CS, Ormsby AR, Cox D, Daly JC, Reid GE, Hatters DM. 2020. Arginine in *C9ORF72* dipolypeptides mediates promiscuous proteome binding and multiple modes of toxicity. *Molecular & Cellular Proteomics* **19**:640–654. DOI: https://doi.org/10.1074/mcp.RA119.001888, PMID: 32086375

Reddy K, Zamiri B, Stanley SYR, Macgregor RB, Pearson CE. 2013. The disease-associated r(GGGGCC)n repeat from the C9orf72 gene forms tract length-dependent uni- and multimolecular RNA G-quadruplex structures. *Journal of Biological Chemistry* **288**:9860–9866. DOI: https://doi.org/10.1074/jbc.C113.452532, PMID: 23423380

Renton AE, Majounie E, Waite A, Simón-Sánchez J, Rollinson S, Gibbs JR, Schymick JC, Laaksovirta H, van Swieten JC, Myllykangas L, Kalimo H, Paetau A, Abramzon Y, Remes AM, Kaganovich A, Scholz SW, Duckworth J, Ding J, Harmer DW, Hernandez DG, et al. 2011. A hexanucleotide repeat expansion in C9ORF72 is the cause of chromosome 9p21-linked ALS-FTD. *Neuron* **72**:257–268. DOI: https://doi.org/10.1016/j.neuron.2011.09.010, PMID: 21944779

Riemslagh FW, Lans H, Seelaar H, Severijnen L, Melhem S, Vermeulen W, Aronica E, Pasterkamp RJ, van Swieten JC, Willemsen R. 2019. HR23B pathology preferentially co-localizes with p62, pTDP-43 and poly-GA in C9ORF72-linked frontotemporal dementia and amyotrophic lateral sclerosis. *Acta Neuropathologica Communications* **7**:39. DOI: https://doi.org/10.1186/s40478-019-0694-6, PMID: 30867060

Rizzu P, Blauwendraat C, Heetveld S, Lynes EM, Castillo-Lizardo M, Dhingra A, Pyz E, Hobert M, Synofzik M, Simón-Sánchez J, Francescatto M, Heutink P. 2016. C9orf72 is differentially expressed in the central nervous system and myeloid cells and consistently reduced in C9orf72, MAPT and GRN mutation carriers. *Acta Neuropathologica Communications* **4**:37. DOI: https://doi.org/10.1186/s40478-016-0306-7, PMID: 27079381

Rossi S, Serrano A, Gerbino V, Giorgi A, Di Francesco L, Nencini M, Bozzo F, Schininà ME, Bagni C, Cestra G, Carrì MT, Achsel T, Cozzolino M. 2015. Nuclear accumulation of mRNAs underlies G4C2-repeat-induced translational repression in a cellular model of C9orf72 ALS. *Journal of Cell Science* **128**:1787–1799. DOI: https://doi.org/10.1242/jcs.165332, PMID: 25788698

Sareen D, O'Rourke JG, Meera P, Muhammad AK, Grant S, Simpkinson M, Bell S, Carmona S, Ornelas L, Sahabian A, Gendron T, Petrucelli L, Baughn M, Ravits J, Harms MB, Rigo F, Bennett CF, Otis TS, Svendsen CN, Baloh RH. 2013. Targeting RNA foci in iPSC-derived motor neurons from ALS patients with a C9ORF72 repeat expansion. *Science Translational Medicine* **5**:208ra149. DOI: https://doi.org/10.1126/scitranslmed.3007529, PMID: 24154603

Scherzinger E, Lurz R, Turmaine M, Mangiarini L, Hollenbach B, Hasenbank R, Bates GP, Davies SW, Lehrach H, Wanker EE. 1997. Huntingtin-encoded polyglutamine expansions form amyloid-like protein aggregates in vitro and in vivo. *Cell* **90**:549–558. DOI: https://doi.org/10.1016/S0092-8674(00)80514-0, PMID: 9267034

Schludi MH, May S, Grässer FA, Rentzsch K, Kremmer E, Küpper C, Klopstock T, Arzberger T, Edbauer D, German Consortium for Frontotemporal Lobar Degeneration, Bavarian Brain Banking Alliance. 2015. Distribution of dipeptide repeat proteins in cellular models and C9orf72 mutation cases suggests link to transcriptional silencing. *Acta Neuropathologica* **130**:537–555. DOI: https://doi.org/10.1007/s00401-015-1450-z, PMID: 26085200

Sellier C, Campanari ML, Julie Corbier C, Gaucherot A, Kolb-Cheynel I, Oulad-Abdelghani M, Ruffenach F, Page A, Ciura S, Kabashi E, Charlet-Berguerand N. 2016. Loss of C9ORF72 impairs autophagy and synergizes with polyQ Ataxin-2 to induce motor neuron dysfunction and cell death. *The EMBO Journal* **35**:1276–1297. DOI: https://doi.org/10.15252/embj.201593350, PMID: 27103069

Shaner NC, Lin MZ, McKeown MR, Steinbach PA, Hazelwood KL, Davidson MW, Tsien RY. 2008. Improving the photostability of bright monomeric orange and red fluorescent proteins. *Nature Methods* **5**:545–551. DOI: https://doi.org/10.1038/nmeth.1209, PMID: 18454154

Shi KY, Mori E, Nizami ZF, Lin Y, Kato M, Xiang S, Wu LC, Ding M, Yu Y, Gall JG, McKnight SL. 2017. Toxic PR_n poly-dipeptides encoded by the *C9orf72* repeat expansio$_n$ block nuclear import and export. *PNAS* **114**:E1111–E1117. DOI: https://doi.org/10.1073/pnas.1620293114, PMID: 28069952

Shi Y, Lin S, Staats KA, Li Y, Chang WH, Hung ST, Hendricks E, Linares GR, Wang Y, Son EY, Wen X, Kisler K, Wilkinson B, Menendez L, Sugawara T, Woolwine P, Huang M, Cowan MJ, Ge B, Koutsodendris N, et al. 2018. Haploinsufficiency leads to neurodegeneration in C9ORF72 ALS/FTD human induced motor neurons. *Nature Medicine* **24**:313–325. DOI: https://doi.org/10.1038/nm.4490, PMID: 29400714

Simón-Sánchez J, Dopper EG, Cohn-Hokke PE, Hukema RK, Nicolaou N, Seelaar H, de Graaf JR, de Koning I, van Schoor NM, Deeg DJ, Smits M, Raaphorst J, van den Berg LH, Schelhaas HJ, De Die-Smulders CE, Majoor-Krakauer D, Rozemuller AJ, Willemsen R, Pijnenburg YA, Heutink P, et al. 2012. The clinical and pathological phenotype of C9ORF72 hexanucleotide repeat expansions. *Brain* **135**:723–735. DOI: https://doi.org/10.1093/brain/awr353, PMID: 22300876

Slomnicki LP, Pietrzak M, Vashishta A, Jones J, Lynch N, Elliot S, Poulos E, Malicote D, Morris BE, Hallgren J, Hetman M. 2016. Requirement of neuronal ribosome synthesis for growth and maintenance of the dendritic tree. *Journal of Biological Chemistry* **291**:5721–5739. DOI: https://doi.org/10.1074/jbc.M115.682161, PMID: 26757818

Solomon DA, Stepto A, Au WH, Adachi Y, Diaper DC, Hall R, Rekhi A, Boudi A, Tziortzouda P, Lee YB, Smith B, Bridi JC, Spinelli G, Dearlove J, Humphrey DM, Gallo JM, Troakes C, Fanto M, Soller M, Rogelj B, et al. 2018. A feedback loop between dipeptide-repeat protein, TDP-43 and karyopherin-α mediates C9orf72-related neurodegeneration. *Brain* **141**:2908–2924. DOI: https://doi.org/10.1093/brain/awy241, PMID: 30239641

Sudria-Lopez E, Koppers M, de Wit M, van der Meer C, Westeneng HJ, Zundel CA, Youssef SA, Harkema L, de Bruin A, Veldink JH, van den Berg LH, Pasterkamp RJ. 2016. Full ablation of C9orf72 in mice causes immune

system-related pathology and neoplastic events but no motor neuron defects. *Acta Neuropathologica* **132**: 145–147. DOI: https://doi.org/10.1007/s00401-016-1581-x, PMID: 27206760

Sullivan PM, Zhou X, Robins AM, Paushter DH, Kim D, Smolka MB, Hu F. 2016. The ALS/FTLD associated protein C9orf72 associates with SMCR8 and WDR41 to regulate the autophagy-lysosome pathway. *Acta Neuropathologica Communications* **4**:51. DOI: https://doi.org/10.1186/s40478-016-0324-5, PMID: 27193190

Suzuki N, Maroof AM, Merkle FT, Koszka K, Intoh A, Armstrong I, Moccia R, Davis-Dusenbery BN, Eggan K. 2013. The mouse C9ORF72 ortholog is enriched in neurons known to degenerate in ALS and FTD. *Nature Neuroscience* **16**:1725–1727. DOI: https://doi.org/10.1038/nn.3566, PMID: 24185425

Swinnen B, Bento-Abreu A, Gendron TF, Boeynaems S, Bogaert E, Nuyts R, Timmers M, Scheveneels W, Hersmus N, Wang J, Mizielinska S, Isaacs AM, Petrucelli L, Lemmens R, Van Damme P, Van Den Bosch L, Robberecht W. 2018. A zebrafish model for C9orf72 ALS reveals RNA toxicity as a pathogenic mechanism. *Acta Neuropathologica* **135**:427–443. DOI: https://doi.org/10.1007/s00401-017-1796-5, PMID: 29302778

Tao Z, Wang H, Xia Q, Li K, Li K, Jiang X, Xu G, Wang G, Ying Z. 2015. Nucleolar stress and impaired stress granule formation contribute to C9orf72 RAN translation-induced cytotoxicity. *Human Molecular Genetics* **24**: 2426–2441. DOI: https://doi.org/10.1093/hmg/ddv005, PMID: 25575510

Tran H, Almeida S, Moore J, Gendron TF, Chalasani U, Lu Y, Du X, Nickerson JA, Petrucelli L, Weng Z, Gao FB. 2015. Differential toxicity of nuclear RNA foci versus dipeptide repeat proteins in a *Drosophila* model of C9ORF72 FTD/ALS. *Neuron* **87**:1207–1214. DOI: https://doi.org/10.1016/j.neuron.2015.09.015, PMID: 26402604

Ugolino J, Ji YJ, Conchina K, Chu J, Nirujogi RS, Pandey A, Brady NR, Hamacher-Brady A, Wang J. 2016. Loss of C9orf72 enhances autophagic activity via deregulated mTOR and TFEB signaling. *PLOS Genetics* **12**:e1006443. DOI: https://doi.org/10.1371/journal.pgen.1006443, PMID: 27875531

Vanneste J, Vercruysse T, Boeynaems S, Sicart A, Van Damme P, Daelemans D, Van Den Bosch L. 2019. C9orf72-generated poly-GR and poly-PR do not directly interfere with nucleocytoplasmic transport. *Scientific Reports* **9**: 15728. DOI: https://doi.org/10.1038/s41598-019-52035-6, PMID: 31673013

Vincenz-Donnelly L, Holthusen H, Körner R, Hansen EC, Presto J, Johansson J, Sawarkar R, Hartl FU, Hipp MS. 2018. High capacity of the endoplasmic reticulum to prevent secretion and aggregation of amyloidogenic proteins. *The EMBO Journal* **37**:337–350. DOI: https://doi.org/10.15252/embj.201695841, PMID: 29247078

Waite AJ, Bäumer D, East S, Neal J, Morris HR, Ansorge O, Blake DJ. 2014. Reduced C9orf72 protein levels in frontal cortex of amyotrophic lateral sclerosis and frontotemporal degeneration brain with the C9ORF72 hexanucleotide repeat expansion. *Neurobiology of Aging* **35**:1779.e5. DOI: https://doi.org/10.1016/j.neurobiolaging.2014.01.016

Wanker EE, Scherzinger E, Heiser V, Sittler A, Eickhoff H, Lehrach H. 1999. Membrane filter assay for detection of amyloid-like polyglutamine-containing protein aggregates. *Methods in Enzymology* **309**:375–386. DOI: https://doi.org/10.1016/s0076-6879(99)09026-6, PMID: 10507036

Wen X, Tan W, Westergard T, Krishnamurthy K, Markandaiah SS, Shi Y, Lin S, Shneider NA, Monaghan J, Pandey UB, Pasinelli P, Ichida JK, Trotti D. 2014. Antisense proline-arginine RAN dipeptides linked to C9ORF72-ALS/FTD form toxic nuclear aggregates that initiate in vitro and in vivo neuronal death. *Neuron* **84**:1213–1225. DOI: https://doi.org/10.1016/j.neuron.2014.12.010, PMID: 25521377

West MW, Wang W, Patterson J, Mancias JD, Beasley JR, Hecht MH. 1999. De novo amyloid proteins from designed combinatorial libraries. *PNAS* **96**:11211–11216. DOI: https://doi.org/10.1073/pnas.96.20.11211, PMID: 10500156

West RJH, Sharpe JL, Voelzmann A, Munro AL, Hahn I, Baines RA, Pickering-Brown S. 2020. Co-expression of C9orf72 related dipeptide-repeats over 1000 repeat units reveals age- and combination-specific phenotypic profiles in *Drosophila*. *Acta Neuropathologica Communications* **8**:158. DOI: https://doi.org/10.1186/s40478-020-01028-y, PMID: 32894207

White MR, Mitrea DM, Zhang P, Stanley CB, Cassidy DE, Nourse A, Phillips AH, Tolbert M, Taylor JP, Kriwacki RW. 2019. C9orf72 poly(PR) Dipeptide repeats disturb biomolecular phase separation and disrupt nucleolar function. *Molecular Cell* **74**:713–728. DOI: https://doi.org/10.1016/j.molcel.2019.03.019

Woerner AC, Frottin F, Hornburg D, Feng LR, Meissner F, Patra M, Tatzelt J, Mann M, Winklhofer KF, Hartl FU, Hipp MS. 2016. Cytoplasmic protein aggregates interfere with nucleocytoplasmic transport of protein and RNA. *Science* **351**:173–176. DOI: https://doi.org/10.1126/science.aad2033, PMID: 26634439

Wolff B, Sanglier JJ, Wang Y. 1997. Leptomycin B is an inhibitor of nuclear export: inhibition of nucleo-cytoplasmic translocation of the human immunodeficiency virus type 1 (HIV-1) Rev protein and Rev-dependent mRNA. *Chemistry & Biology* **4**:139–147. DOI: https://doi.org/10.1016/S1074-5521(97)90257-X, PMID: 9190288

Xu Z, Poidevin M, Li X, Li Y, Shu L, Nelson DL, Li H, Hales CM, Gearing M, Wingo TS, Jin P. 2013. Expanded GGGGCC repeat RNA associated with amyotrophic lateral sclerosis and frontotemporal dementia causes neurodegeneration. *PNAS* **110**:7778–7783. DOI: https://doi.org/10.1073/pnas.1219643110, PMID: 23553836

Yamakawa M, Ito D, Honda T, Kubo K, Noda M, Nakajima K, Suzuki N. 2015. Characterization of the dipeptide repeat protein in the molecular pathogenesis of c9FTD/ALS. *Human Molecular Genetics* **24**:1630–1645. DOI: https://doi.org/10.1093/hmg/ddu576, PMID: 25398948

Yang M, Liang C, Swaminathan K, Herrlinger S, Lai F, Shiekhattar R, Chen JF. 2016. A C9ORF72/SMCR8-containing complex regulates ULK1 and plays a dual role in autophagy. *Science Advances* **2**:e1601167. DOI: https://doi.org/10.1126/sciadv.1601167, PMID: 27617292

Zhang YJ, Jansen-West K, Xu YF, Gendron TF, Bieniek KF, Lin WL, Sasaguri H, Caulfield T, Hubbard J, Daughrity L, Chew J, Belzil VV, Prudencio M, Stankowski JN, Castanedes-Casey M, Whitelaw E, Ash PE, DeTure M, Rademakers R, Boylan KB, et al. 2014. Aggregation-prone c9FTD/ALS poly(GA) RAN-translated proteins cause

neurotoxicity by inducing ER stress. *Acta Neuropathologica* **128**:505–524. DOI: https://doi.org/10.1007/s00401-014-1336-5, PMID: 25173361

Zhang K, Donnelly CJ, Haeusler AR, Grima JC, Machamer JB, Steinwald P, Daley EL, Miller SJ, Cunningham KM, Vidensky S, Gupta S, Thomas MA, Hong I, Chiu SL, Huganir RL, Ostrow LW, Matunis MJ, Wang J, Sattler R, Lloyd TE, et al. 2015. The C9orf72 repeat expansion disrupts nucleocytoplasmic transport. *Nature* **525**:56–61. DOI: https://doi.org/10.1038/nature14973, PMID: 26308891

Zhang YJ, Gendron TF, Grima JC, Sasaguri H, Jansen-West K, Xu YF, Katzman RB, Gass J, Murray ME, Shinohara M, Lin WL, Garrett A, Stankowski JN, Daughrity L, Tong J, Perkerson EA, Yue M, Chew J, Castanedes-Casey M, Kurti A, et al. 2016. C9ORF72 poly(GA) aggregates sequester and impair HR23 and nucleocytoplasmic transport proteins. *Nature Neuroscience* **19**:668–677. DOI: https://doi.org/10.1038/nn.4272, PMID: 26998601

Zhang K, Daigle JG, Cunningham KM, Coyne AN, Ruan K, Grima JC, Bowen KE, Wadhwa H, Yang P, Rigo F, Taylor JP, Gitler AD, Rothstein JD, Lloyd TE. 2018a. Stress granule assembly disrupts nucleocytoplasmic transport. *Cell* **173**:958–971. DOI: https://doi.org/10.1016/j.cell.2018.03.025, PMID: 29628143

Zhang YJ, Gendron TF, Ebbert MTW, O'Raw AD, Yue M, Jansen-West K, Zhang X, Prudencio M, Chew J, Cook CN, Daughrity LM, Tong J, Song Y, Pickles SR, Castanedes-Casey M, Kurti A, Rademakers R, Oskarsson B, Dickson DW, Hu W, et al. 2018b. Poly(GR) impairs protein translation and stress granule dynamics in C9orf72-associated frontotemporal dementia and amyotrophic lateral sclerosis. *Nature Medicine* **24**:1136–1142. DOI: https://doi.org/10.1038/s41591-018-0071-1, PMID: 29942091

Zhu Q, Jiang J, Gendron TF, McAlonis-Downes M, Jiang L, Taylor A, Diaz Garcia S, Ghosh Dastidar S, Rodriguez MJ, King P, Zhang Y, La Spada AR, Xu H, Petrucelli L, Ravits J, Da Cruz S, Lagier-Tourenne C, Cleveland DW. 2020. Reduced C9ORF72 function exacerbates gain of toxicity from ALS/FTD-causing repeat expansion in C9orf72. *Nature Neuroscience* **23**:615–624. DOI: https://doi.org/10.1038/s41593-020-0619-5, PMID: 32284607

Zu T, Liu Y, Bañez-Coronel M, Reid T, Pletnikova O, Lewis J, Miller TM, Harms MB, Falchook AE, Subramony SH, Ostrow LW, Rothstein JD, Troncoso JC, Ranum LP. 2013. RAN proteins and RNA foci from antisense transcripts in C9ORF72 ALS and frontotemporal dementia. *PNAS* **110**:E4968–E4977. DOI: https://doi.org/10.1073/pnas.1315438110, PMID: 24248382